NASA/CR—2014-218107

Modeling Sound Propagation Through Non-Axisymmetric Jets

Stewart J. Leib
Ohio Aerospace Institute, Brook Park, Ohio

March 2014

NASA STI Program . . . in Profile

Since its founding, NASA has been dedicated to the advancement of aeronautics and space science. The NASA Scientific and Technical Information (STI) program plays a key part in helping NASA maintain this important role.

The NASA STI Program operates under the auspices of the Agency Chief Information Officer. It collects, organizes, provides for archiving, and disseminates NASA's STI. The NASA STI program provides access to the NASA Aeronautics and Space Database and its public interface, the NASA Technical Reports Server, thus providing one of the largest collections of aeronautical and space science STI in the world. Results are published in both non-NASA channels and by NASA in the NASA STI Report Series, which includes the following report types:

- TECHNICAL PUBLICATION. Reports of completed research or a major significant phase of research that present the results of NASA programs and include extensive data or theoretical analysis. Includes compilations of significant scientific and technical data and information deemed to be of continuing reference value. NASA counterpart of peer-reviewed formal professional papers but has less stringent limitations on manuscript length and extent of graphic presentations.

- TECHNICAL MEMORANDUM. Scientific and technical findings that are preliminary or of specialized interest, e.g., quick release reports, working papers, and bibliographies that contain minimal annotation. Does not contain extensive analysis.

- CONTRACTOR REPORT. Scientific and technical findings by NASA-sponsored contractors and grantees.

- CONFERENCE PUBLICATION. Collected papers from scientific and technical conferences, symposia, seminars, or other meetings sponsored or cosponsored by NASA.

- SPECIAL PUBLICATION. Scientific, technical, or historical information from NASA programs, projects, and missions, often concerned with subjects having substantial public interest.

- TECHNICAL TRANSLATION. English-language translations of foreign scientific and technical material pertinent to NASA's mission.

Specialized services also include creating custom thesauri, building customized databases, organizing and publishing research results.

For more information about the NASA STI program, see the following:

- Access the NASA STI program home page at *http://www.sti.nasa.gov*

- E-mail your question to *help@sti.nasa.gov*

- Fax your question to the NASA STI Information Desk at 443–757–5803

- Phone the NASA STI Information Desk at 443–757–5802

- Write to:
  STI Information Desk
  NASA Center for AeroSpace Information
  7115 Standard Drive
  Hanover, MD 21076–1320

NASA/CR—2014-218107

Modeling Sound Propagation Through Non-Axisymmetric Jets

Stewart J. Leib
Ohio Aerospace Institute, Brook Park, Ohio

Prepared under Contract NNC07BA13B

National Aeronautics and
Space Administration

Glenn Research Center
Cleveland, Ohio 44135

March 2014

Acknowledgments

This work was supported by the NASA Fundamental Aeronautics Program High-Speed Project. The author would like to thank Mr. E. Brian Fite and Dr. James Bridges for their support and Mr. Daniel Ingraham for his comments on an early draft of this report.

This report contains preliminary findings, subject to revision as analysis proceeds.

This work was sponsored by the Fundamental Aeronautics Program at the NASA Glenn Research Center.

Level of Review: This material has been technically reviewed by NASA technical management OR expert reviewer(s).

Available from

NASA Center for Aerospace Information
7115 Standard Drive
Hanover, MD 21076–1320

National Technical Information Service
5301 Shawnee Road
Alexandria, VA 22312

Available electronically at http://www.sti.nasa.gov

Modeling Sound Propagation Through Non-Axisymmetric Jets

Stewart J. Leib
Ohio Aerospace Institute
Brook Park, Ohio 44142

Abstract

A method for computing the far-field adjoint Green's function of the generalized acoustic analogy equations under a locally parallel mean flow approximation is presented. The method is based on expanding the mean-flow-dependent coefficients in the governing equation and the scalar Green's function in truncated Fourier series in the azimuthal direction and a finite difference approximation in the radial direction in circular cylindrical coordinates. The combined spectral/finite difference method yields a highly banded system of algebraic equations that can be efficiently solved using a standard sparse system solver. The method is applied to test cases, with mean flow specified by analytical functions, corresponding to two noise reduction concepts of current interest: the offset jet and the fluid shield. Sample results for the Green's function are given for these two test cases and recommendations made as to the use of the method as part of a RANS-based jet noise prediction code.

1.0 Introduction

Exhaust system noise emission continues to be an issue for commercial and military aircraft and is, therefore, the subject of ongoing research efforts as to its understanding, prediction and reduction. National and international regulations are imposing significant limitations on the noise footprint of aircraft operations, which are driving the development of noise-reduction concepts. Nearly all of these concepts involve the use of non-circular geometries to attempt to reduce overall noise emissions, or tailor the directivity characteristics in a desired manner. Robust and reliable prediction tools are needed to assess the noise-reduction potential of proposed concepts. In addition, since each concept typically involves numerous parametric options, noise prediction codes that can provide results relatively quickly, i.e., in a time period short enough to include them in the design process, are especially needed. Although progress continues to be made on direct numerical simulation of noise from turbulent flows, such calculations are still much too time consuming to be used in the design and optimization processes for new aircraft exhaust systems and reduced-order methods, therefore, are needed.

Most practical noise prediction codes are based on an acoustic analogy, wherein the sound-generating turbulent flow is replaced by a set of equivalent sources with the sound propagating through a specified base flow. The acoustic analogy approach was pioneered by Lighthill (Refs. 1 and 2). Subsequent formulations, such as that Lilley (Ref. 3), explicitly account for mean flow interaction effects in the linear differential wave operator. The JeNo code (Refs. 4 and 5) is based on the Lilley (Ref. 3) analogy and is an example of the type of statistically based prediction code which can be used for parametric studies in round jets.

Goldstein (Ref. 6) showed that the Navier-Stokes equations can be rewritten as a set of `base' flow equations plus a formally linear (about the base flow) set of equations for the 'residual' component (the difference between the total and base flow), and that the latter can be put into the form of the linearized Navier-Stokes equations with source terms whose strengths are represented by a generalized Reynolds stress. The general formulation of (Ref. 6) was used by Goldstein and Leib (Ref. 7) to develop an acoustic analogy-based approach for jet noise predictions from information about the turbulence. The method was applied to round, unheated jets in References 7 and 8 and the results showed good agreement with experimental data for subsonic and moderately supersonic jets at all polar angles throughout the range of interest.

Implementations of acoustic analogy formulations typically rely on the computation of a Green's function to describe sound propagation through the base flow coupled with models for the nominal source terms arising from the particular analogy formulation being used. For an axisymmetric, locally parallel, mean flow the problem for the Green's function can be reduced to solving an uncoupled set of second-order ordinary differential equations for its azimuthal Fourier modes. For non-axisymmetric jets, such reduction is not generally possible and, since most of the computational expense of acoustic analogy based noise prediction methods is incurred in computing the Green's function, predictions for non-axisymmetric jets are generally significantly more time consuming than those for axisymmetric ones.

A reduced-order model for obtaining the Green's function for certain classes of non-axisymmetric jets was presented in (Ref. 9). The approach uses a conformal mapping of the level surfaces of mean streamwise velocity and sound speed (assumed to be coincident) and their orthogonal curves to a semi-infinite periodic strip. The Green's function can then be solved in terms of its Fourier modes (in the transformed plane), but the latter are now coupled, owing to the 'azimuthal' dependence of the Jacobian of the transformation. The method was applied to a set of rectangular jets (the Extensible Rectangular Nozzle (ERN) System (Ref. 10)) using a mapping to cylindrical elliptical coordinates along with the hybrid source model developed in Reference 8. Results from low-speed flow surveys of the jet plumes, carried out by Zaman (Ref. 11), were used to scale the various source components of the model. Extensive PIV flow measurements of these jets were later made by Bridges and Wernet (Ref. 12). Comparisons of the results of noise calculations using this method with data taken in the Small Hot Jet Acoustic Rig (SHJAR) at NASA Glenn (Ref. 13) showed that the model was capable of predicting the overall azimuthal directivity characteristics of these non-axisymmetric jets.

The conformal mapping based method provides a reduced-order model for obtaining the Green's function with computational resources comparable to those required for a round jet, but it is has some limitations as to the types of mean flows that can be treated. A number of the noise reduction concepts currently being considered are not amenable to the conformal mapping method and it is desirable to have a more general method that can treat a wider range of geometries.

In this report, we present a more general method for computing the Green's function of the acoustic analogy equations for a locally parallel mean flow that could potentially be used for most of the noise reduction concepts currently of interest to NASA. The method relies on a Fourier series representation of the azimuthal variation of the mean flow dependent coefficients appearing in the governing equation for the Green's function, and solves for the latter in terms of its own azimuthal Fourier components. As in the conformal mapping based approach (and to a potentially much greater extent), the equations for the azimuthal Fourier modes of the Green's function are coupled in the present method, requiring solution of a (possibly quite large) system of simultaneous ordinary differential equations. One purpose of this report is to demonstrate the use of the method on some relatively generic non-axisymmetric jets and determine the feasibility of using it in the context of a noise prediction scheme for non-axisymmetric jets.

The overall plan of the paper is as follows. In Section 2.0 the equations and boundary conditions governing the far-field adjoint Green's function for a locally parallel mean flow are given. The numerical method used to solve for the azimuthal Fourier modes of the Green's function is described in Section 3.0. In Section 4.0 results are presented using this method for a round jet and the results compared with those from an existing, established, round jet code. Two non-axisymmetric test cases are then described in Section 4.0. These test cases are meant to be representative of two noise reduction concepts of interest to NASA. Results from these test cases are presented in Section 5.0. In Section 6.0 we summarize the results and provide recommendations for the application of this method to noise predictions in non-axisymmetric jets.

2.0 Governing Equation

For a locally parallel mean flow, the components of the adjoint vector Green's function of the acoustic analogy equations can be expressed in terms of a single scalar function that, for observer locations in the far field, satisfies (Refs. 7 and 8)

$$\frac{\partial}{\partial y_j}\frac{\widetilde{c^2}(\boldsymbol{y}_T)}{\left[1-M(\boldsymbol{y}_\perp)\cos\theta\right]^2}\frac{\partial g(\boldsymbol{y}_T;\varphi,\theta:\omega)}{\partial y_j} + \omega^2\left\{1-\frac{\left(\widetilde{c^2}(\boldsymbol{y}_T)/c_\infty^2\right)\cos^2\theta}{\left[1-M(\boldsymbol{y}_\perp)\cos\theta\right]^2}\right\}g(\boldsymbol{y}_T;\varphi,\theta:\omega)=0; \quad j=2,3, \tag{2.1}$$

where $\boldsymbol{y} = (y_1, \boldsymbol{y}_T)$ are Cartesian coordinates, with y_1 being in the direction of the mean flow and $\boldsymbol{y}_T = (y_2, y_3)$ the cross flow coordinates, $\widetilde{c^2}(\boldsymbol{y}_T)$ is the mean sound speed profile, whose ambient value is denoted as c_∞^2, $M(\boldsymbol{y}_T) = U(\boldsymbol{y}_T)/c_\infty$ is the acoustic Mach number profile corresponding to the mean axial velocity profile $U(\boldsymbol{y}_T)$, ω is the radian frequency and θ,φ are the observer polar and azimuthal angles, defined as $\theta = \cos^{-1}\left(x_1 \Big/ \left(x_1^2+x_2^2+x_3^2\right)^{1/2}\right)$ and $\varphi = \tan^{-1}\left(x_3/x_2\right)$, respectively with $\boldsymbol{x} = (x_1, x_2, x_3)$ the Cartesian coordinates of the observer.

The solution is subject to the far-field boundary condition

$$g(\boldsymbol{y}_\perp;\varphi,\theta:\omega) \to \frac{(\omega/c_\infty)^2 e^{-i\omega/c_\infty \sin\theta\, y_\perp \cos(\varphi-\varphi_0)} e^{i\pi/4}}{2(2\pi)^2\sqrt{2\pi\sin\theta\,\omega/c_\infty}} + \text{outgoing waves}, \tag{2.2}$$

as $y_T = |\boldsymbol{y}_T| \to \infty$, where $\varphi_0 = \tan^{-1}(y_3/y_2)$, together with appropriate boundedness and/or continuity conditions.

We express (2.1) in terms of the polar coordinates (y_T, φ_0),

$$\frac{\partial^2 g}{\partial y_T^2} + \frac{1}{y_T}\frac{\partial g}{\partial y_T} + \frac{1}{y_T^2}\frac{\partial^2 g}{\partial \varphi_0^2} + \mathcal{R}\frac{\partial g}{\partial y_T} + \mathcal{T}\frac{\partial g}{y_T \partial \varphi_0} + \omega^2 \mathcal{H} g = 0, \tag{2.3}$$

where

$$\mathcal{R}(y_T,\varphi_0) = \left\{\frac{2\cos\theta}{\left[1-M(\boldsymbol{y}_T)\cos\theta\right]}\frac{\partial M(\boldsymbol{y}_T)}{\partial y_T} + \frac{1}{\widetilde{c^2}(\boldsymbol{y}_T)}\frac{\partial \widetilde{c^2}(\boldsymbol{y}_T)}{\partial y_T}\right\}, \tag{2.4}$$

$$\mathcal{T}(y_T,\varphi_0) = \left\{\frac{2\cos\theta}{\left[1-M(\boldsymbol{y}_T)\cos\theta\right]}\frac{\partial M(\boldsymbol{y}_T)}{y_T\partial \varphi_0} + \frac{1}{\widetilde{c^2}(\boldsymbol{y}_T)}\frac{\partial \widetilde{c^2}(\boldsymbol{y}_T)}{y_T\partial \varphi_0}\right\}, \tag{2.5}$$

and

$$\mathcal{H}(y_T,\varphi_0) = \left\{\frac{\left[1-M(\boldsymbol{y}_T)\cos\theta\right]^2}{\widetilde{c^2}(\boldsymbol{y}_T)} - \frac{\cos^2\theta}{c_\infty^2}\right\}. \tag{2.6}$$

For applications where the mean flow is not too far from axisymmetric, the coefficients, (2.4) to (2.6), of Equation (2.3) can be reasonably well approximated by a relatively small number of terms, say L, of their Fourier series expansions

$$\mathcal{R}(y_T,\varphi_0)=\sum_{l=-L}^{L}\mathcal{R}_l(y_T)e^{il\varphi_0};\quad \mathcal{I}(y_T,\varphi_0)=\sum_{l=-L}^{L}\mathcal{I}_l(y_T)e^{il\varphi_0};\quad \mathcal{H}(y_T,\varphi_0)=\sum_{l=-L}^{L}\mathcal{H}_l(y_T)e^{il\varphi_0} \tag{2.7}$$

Using (2.7) in (2.3), the solution for the far-field scalar adjoint Green's function can be sought in terms of the coefficients of its truncated Fourier series,

$$g(y_\perp,\varphi_0;\varphi,\theta:\omega)\approx\sum_{n=-N}^{N}g_n(y_\perp;\varphi,\theta:\omega)e^{in\varphi_0} \tag{2.8}$$

from

$$\begin{aligned}\frac{\partial^2 g_n}{\partial {y_T}^2}+\frac{1}{y_T}\frac{\partial g_n}{\partial y_T}-\frac{n^2}{{y_T}^2}g_n+\sum_{l=-L}^{L}\mathcal{R}_l\frac{\partial g_{n-l}}{\partial y_T}+\\ +\sum_{l=-L}^{L}\mathcal{I}_l\frac{i}{y_T}(n-l)g_{n-l}+\omega^2\sum_{l=-L}^{L}\mathcal{H}_l g_{n-l}=0\quad;\ -N\le n\le N\end{aligned}, \tag{2.9}$$

where $L \le N$.

The far-field boundary conditions on the Fourier modes, g_n, are obtained from (2.2) as

$$g_n(y_\perp;\varphi,\theta:\omega)\to\frac{(\omega/c_\infty)^2 e^{i\pi/4}}{4(2\pi)^2\sqrt{2\pi\sin\theta\,\omega/c_\infty}}e^{-in(\varphi+\pi/2)}+\text{outgoing waves as } y_T\to\infty, \tag{2.10}$$

where $H_n^{(2)}$ is the Hankel function of the second kind.

To eliminate the outgoing wave component of the far-field boundary condition (2.10) (whose amplitude is unknown), a Robin-type condition is imposed

$$\frac{dg_n}{dy_T}+\kappa_n g_n\to\left(\frac{d}{dy_T}+\kappa_n\right)\frac{(\omega/c_\infty)^2 e^{i\pi/4}}{4(2\pi)^2\sqrt{2\pi\sin\theta\,\omega/c_\infty}}e^{-in(\varphi+\pi/2)}H_n^{(2)}\left(\frac{\omega}{c_\infty}y_T\sin\theta\right)=\Gamma_n(y_T), \tag{2.11}$$

as $y_T\to\infty$

where

$$\kappa_n=\frac{-\omega\cos\theta}{c_\infty}\frac{H_n^{(1)\prime}\left(\frac{\omega}{c_\infty}y_T\sin\theta\right)}{H_n^{(1)}\left(\frac{\omega}{c_\infty}y_T\sin\theta\right)}, \tag{2.12}$$

$H_n^{(1)}$ is the Hankel function of the first kind of order n, and the prime denotes differentiation with respect to the argument.

Near the origin, a Frobenius analysis shows that appropriate inner boundary conditions are

$$\begin{aligned}&g_n(0;\varphi,\theta:\omega)=0, n\ne 0\\ &\frac{dg_0(0;\varphi,\theta:\omega)}{dy_T}=0\end{aligned}. \tag{2.13}$$

3.0 Numerical Methods

For numerical solution of the Fourier components of the far-field scalar adjoint Green's function, the radial derivatives in the governing Equations (2.9), far-field boundary condition (2.11) and the second starting condition of (2.13) are replaced by second-order central differences, and a system of algebraic equations for the Fourier modes of the Green's function at discrete grid points is formed.

The domain is discretized using a uniform grid size, Δ, so that

$$y_T^{j+1} - y_T^j = \Delta \;\; ; \;\; j = 1, J-1 , \tag{3.1}$$

and the Fourier components of the solution at the discrete grid points are represented by g_n^j.

Then the initial (or starting) conditions (2.13) become

$$\begin{aligned} & g_n^1 = 0, n \neq 0 \\ & -g_0^2 + g_0^1 = 0 \end{aligned}, \tag{3.2}$$

the governing Equations (2.9) become

$$\sum_{l=-L}^{L} \mathcal{B}_l^j g_{n-l}^{j-1} + \sum_{l=-L}^{L} \mathcal{A}_l^{j,n} g_{n-l}^j + \sum_{l=-L}^{L} \mathcal{C}_l^j g_{n-l}^{j+1} = 0; \quad 2 \le j \le J-1, \;\; -N \le n \le N , \tag{3.3}$$

where

$$\mathcal{B}_l^j = \left[\delta_{l,0} \left(1 - \frac{\Delta}{2 y_T} \right) - \frac{\Delta}{2} \mathcal{R}_l^j \right] , \tag{3.4}$$

$$\mathcal{A}_l^{j,n} = \left[-\delta_{l,0} \left(2 + \frac{n^2 \Delta^2}{{y_T}^2} \right) + \mathcal{T}_l^j \frac{\Delta^2}{y_T} i(n-1) + \mathcal{H}_l^j \omega^2 \Delta^2 \right], \tag{3.5}$$

$$\mathcal{C}_l^j = \left[\delta_{l,0} \left(1 + \frac{\Delta}{2 y_T} \right) + \frac{\Delta}{2} \mathcal{R}_l^j \right], \tag{3.6}$$

and the far-field boundary condition (2.11) becomes

$$\left(-1 + \frac{\Delta \kappa_n^{J-1/2}}{2} \right) g_n^{J-1} + \left(1 + \frac{\Delta \kappa_n^{J-1/2}}{2} \right) g_n^J = \Delta \Gamma_n^{J-1/2} \quad . \tag{3.7}$$

The system of equations is written in matrix form as

$$\boldsymbol{B}_j \tilde{\boldsymbol{g}}^{j-1} + \boldsymbol{A}_j \tilde{\boldsymbol{g}}^j + \boldsymbol{C}_j \tilde{\boldsymbol{g}}^{j+1} = \boldsymbol{\Gamma}_j ; \;\; j = 1, J \tag{3.8}$$

where $\boldsymbol{A}_j$, $\boldsymbol{B}_j$, $\boldsymbol{C}_j$ are $(2N+1) \times (2N+1)$ matrices, with $\boldsymbol{B}_1 = \boldsymbol{C}_J = \boldsymbol{0}$,

$$\boldsymbol{g}^j = \begin{Bmatrix} g^j_{-N} \\ g^j_{-N+1} \\ \cdot \\ \cdot \\ \cdot \\ g^j_n \\ \cdot \\ \cdot \\ \cdot \\ g^j_N \end{Bmatrix}, \tag{3.9}$$

is a $(2N + 1)$-length vector. The system is of block-tridiagonal form, and can be efficiently solved using a sparse system algorithm.

4.0 Validation and Test Cases

As a validation case for the computer code written to implement this method, a round jet is considered and results are compared with those from an established noise prediction code for round jets (Refs. 7 and 8). Two non-circular test cases are then presented that will be used as applications of the method. They are meant to be representative of two noise reduction concepts of current interest: the offset jet and the fluid shield.

4.1 Round Jet

A round jet with mean acoustic Mach number profile

$$M(r) = M_C e^{-\alpha r^2} \ , \tag{4.1}$$

where the radial coordinate is now denoted by $r = y_T$, and uniform mean sound speed profile, $\widetilde{c^2}(r) \equiv c_\infty^2$, was considered as the validation case for the code. Calculations were carried out for $M_C = 0.5$ and $\alpha = 1$.

Figure 1 shows comparisons of the results computed for this case using the new code with those of the established round jet code for a polar angle $\theta = 60°$ at a range of Strouhal numbers, $\mathrm{St} = \dfrac{\omega D}{2\pi U_J}$ and several azimuthal observer angles at a radial source location of one-half. Figure 2 shows corresponding results for $\theta = 30°$. Results at other radial source locations are generally similar. The results are in good agreement, although there begins to be some discrepancy as the Strouhal number increases. Increasing the number of Fourier modes used to compute the solution can be shown to ameliorate this discrepancy.

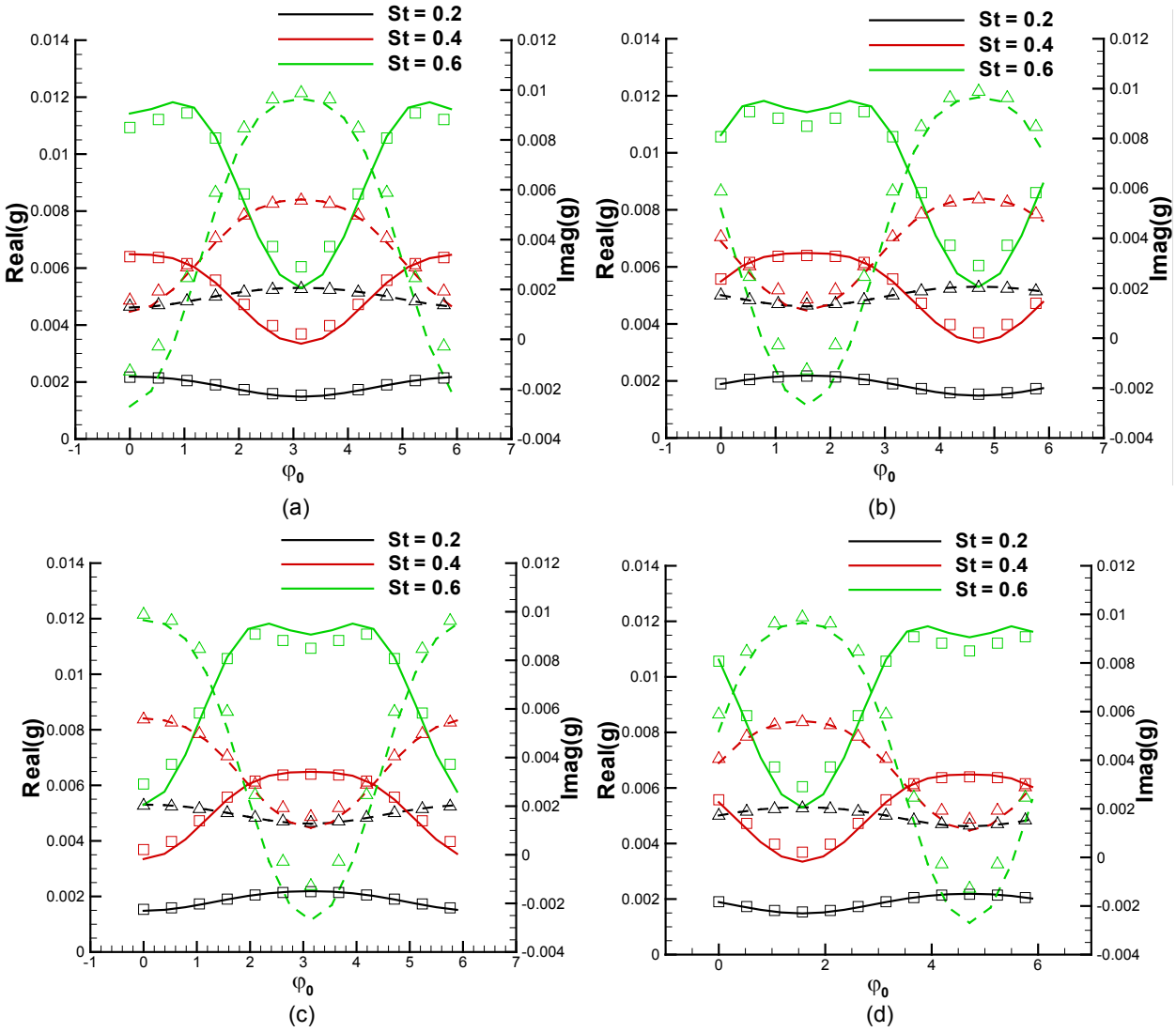

Figure 1.—Comparisons of results for the far-field adjoint Green's function versus azimuthal location in a round jet at $\theta = 60°$, $r = 0.5$. (a) $\varphi = 0$, (b) $\varphi = 90$, (c) $\varphi = 180$, (d) $\varphi = 270$. Results from code of Reference 7 and 8 (Curves), from current code (Symbols). Re(g) solid lines and squares, Im(g) dashed lines and triangles.

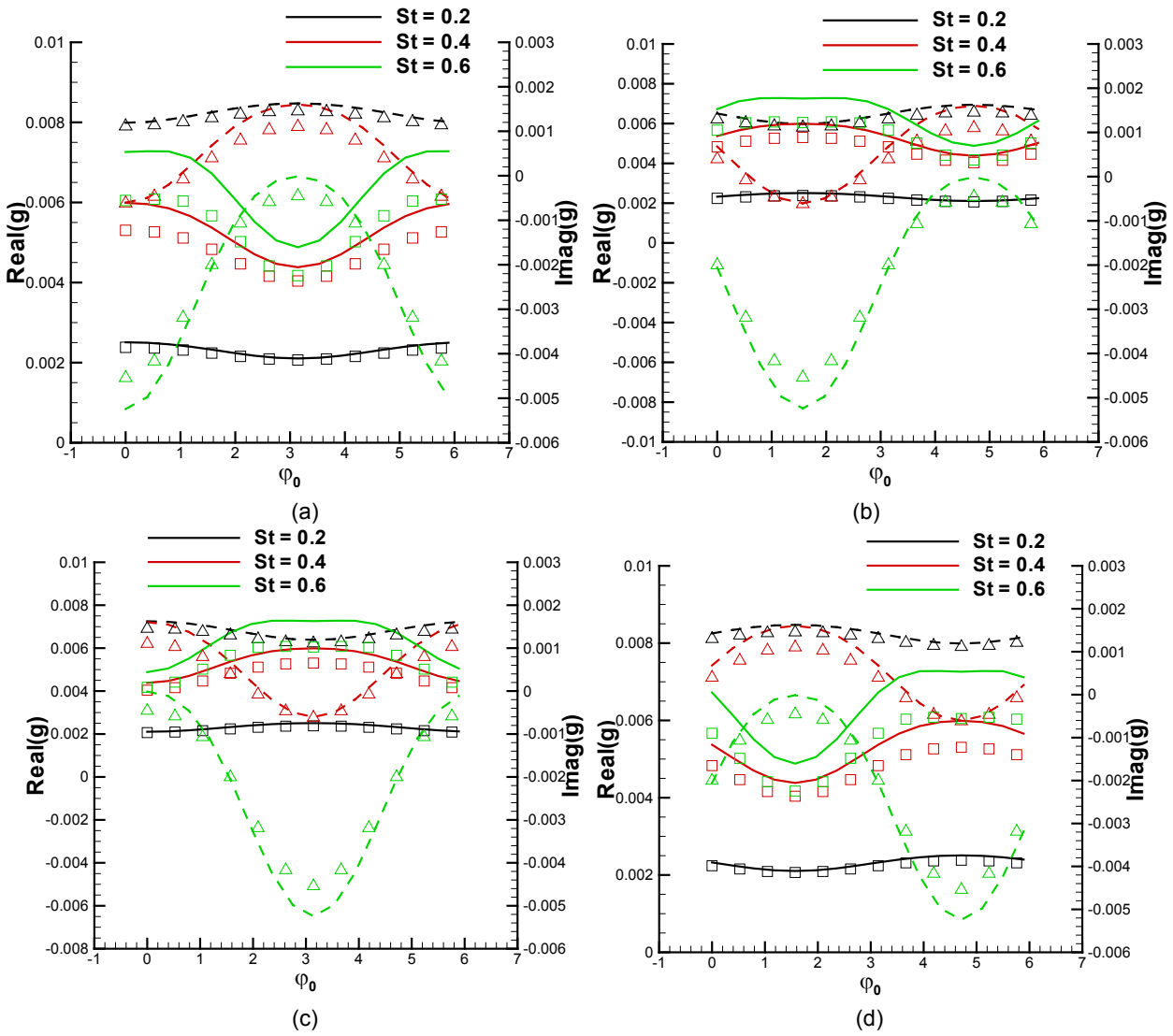

Figure 2.—Comparisons of results for the far-field adjoint Green's function versus azimuthal location in a round jet at θ = 30°, *r* = 0.5. (a) φ = 0, (b) φ = 90, (c) φ = 180, (d) φ = 270. Results from code of References 7 and 8 (Curves), from current code (Symbols).Re(*g*) solid lines and squares, Im(*g*)dashed lines and triangles.

In the next two subsections, we present the non-circular jet test cases used as example applications of the code.

4.2 The Offset Jet

The first non-circular geometry considered is that of the offset jet. As a model for the mean flow for this case, we take the mean acoustic Mach number profile to be

$$M(r,\varphi) = M_C e^{-(1+\alpha-2\alpha\cos\varphi)r^2} \quad . \tag{4.2}$$

Figure 3 shows mean acoustic Mach number contours for this profile with $M_C = 0.5$, $\alpha = 0.8$. The mean flow consists of a thick and a thin side and experiments have found significant asymmetry in the sound field emitted from jets of this form.

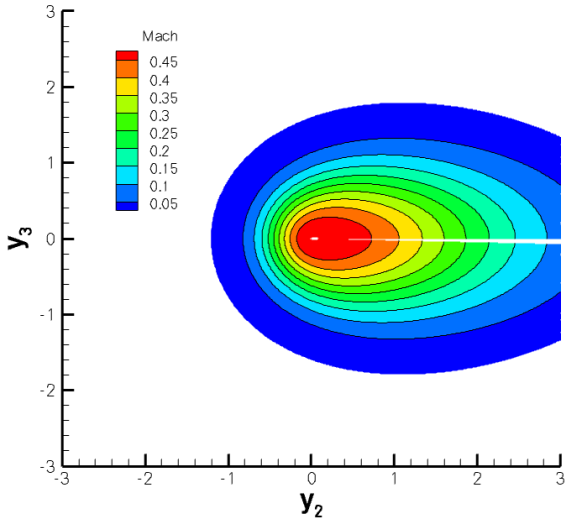

Figure 3.—Mean acoustic Mach number contours for the offset jet.

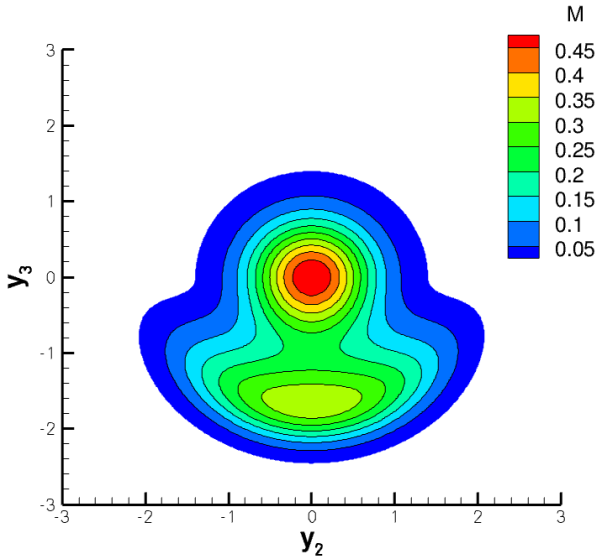

Figure 4.—Mean acoustic Mach number contours for the fluid shield.

4.3 Fluid Shield

The second non-circular case considered is the so-called fluid shield. In this geometry, a round core flow is partially surrounded by a secondary stream, with the latter intended to shield the region below it by refracting sound. A model for the mean flow for this configuration is

$$M(r,\varphi) = M_C\left[e^{-ar^2} + br^2 e^{-c(r-1)^4} g(\varphi)\right]$$
$$g(\varphi) = \begin{cases} 0, & 0 \le \varphi < \pi \\ \sin^2\varphi, & \pi \le \varphi < 2\pi \end{cases} \quad . \tag{4.3}$$

Figure 4 shows the mean acoustic Mach number contours for this profile for $M_C = 0.5$, $a = 2.0$, $b = 0.3$, $c = 1.0$.

5.0 Results

In this section we present results for the two noncircular jet test cases considered as example applications of the method. For each test case, we first show results demonstrating the Fourier series representation of the mean flow terms appearing in the governing Equation (2.3). The Fourier coefficients of the mean flow terms, (2.4) to (2.6), were computed at relatively high resolution (2048 points) to obtain accurate values of the coefficients using the routine FFTW. Subsets of these coefficients were then used in (2.7) to reconstruct these functions for different choices of L and the results compared with the full quantities. We then present results for the Green's function using these Fourier series representations of the coefficients. For these calculations, we have taken the mean sound speed to be uniform (equal to its ambient value) and, therefore, for polar angles of $\theta = 90°$ the effect of the mean flow vanishes and the magnitude of the scalar adjoint Green's function is an axisymmetric function of $\varphi_0 - \varphi$. It has been verified that results from the code give this behavior for both test cases, but, since the emphasis here is on the asymmetry produced by the mean flow field, we only present results at polar angles of 30° and 60° (relative to the downstream jet axis). Calculations were carried out using sixteen modes ($N = 16$) for the Green's function, a step size $\Delta = 0.005$ and a maximum radial extent for the computational domain of 5.0. Testing was carried out to verify that these numerical parameters are sufficient for the two test cases of interest.

Results are presented showing the effect of the number of Fourier modes used to represent the mean flow terms on the numerical solution for the Green's function. In particular, we demonstrate that numerical results for the Green's function converge (that is they are unchanged with increasing number of mean flow modes) for a reasonable number of mean flow modes for these two test cases.

We note that the high-frequency asymptotic solution (Ref. 14) suggests that the scaled Green's function, $\omega^{-3/2}|g|$, should become independent of frequency as $\omega \to \infty$. As another check on the numerical results for the Green's function, we plot this quantity for increasing Strouhal number and verify that it has this form.

Results are then presented showing the azimuthal directivity of the Green's function as a function of the Strouhal number, at polar observation angles of 30° and 60° to the jet axis.

In jet noise calculations based on an acoustic analogy formulation, prediction results are usually obtained by evaluating a formula derived for the far-field acoustic spectrum. This formula involves the Green's function, and its derivatives, in combination with Doppler factors multiplying the various components of the Reynolds stress auto-covariance tensor, which are the source terms (Refs. 7 and 8). Prediction of the noise characteristics of a particular nozzle configuration requires the use of this full formula. However, as a rough estimate of the potential noise-shielding effects of non-axisymmetric mean flows, the directivity of the magnitude of the adjoint Green's function itself can be used as a guide. Therefore, in the final set of results presented, we examine the computed results for directivity of the magnitude of the adjoint Green's for a selected set of source locations in an attempt to gain some physical insight into the potential noise-shielding properties of the mean flows for these two test cases.

5.1 Offset Jet

5.1.1 Fourier Representation of the Mean Flow Terms

In this section we present results for the Fourier series representation of the mean flow terms appearing in the governing equations for the case of the offset jet. Figure 5 shows contour plots in the cross flow, (y_2, y_3), plane of the mean flow terms, $\mathcal{R}$, $\mathcal{J}$, $\mathcal{H}$, in Equation (2.3) for this case.

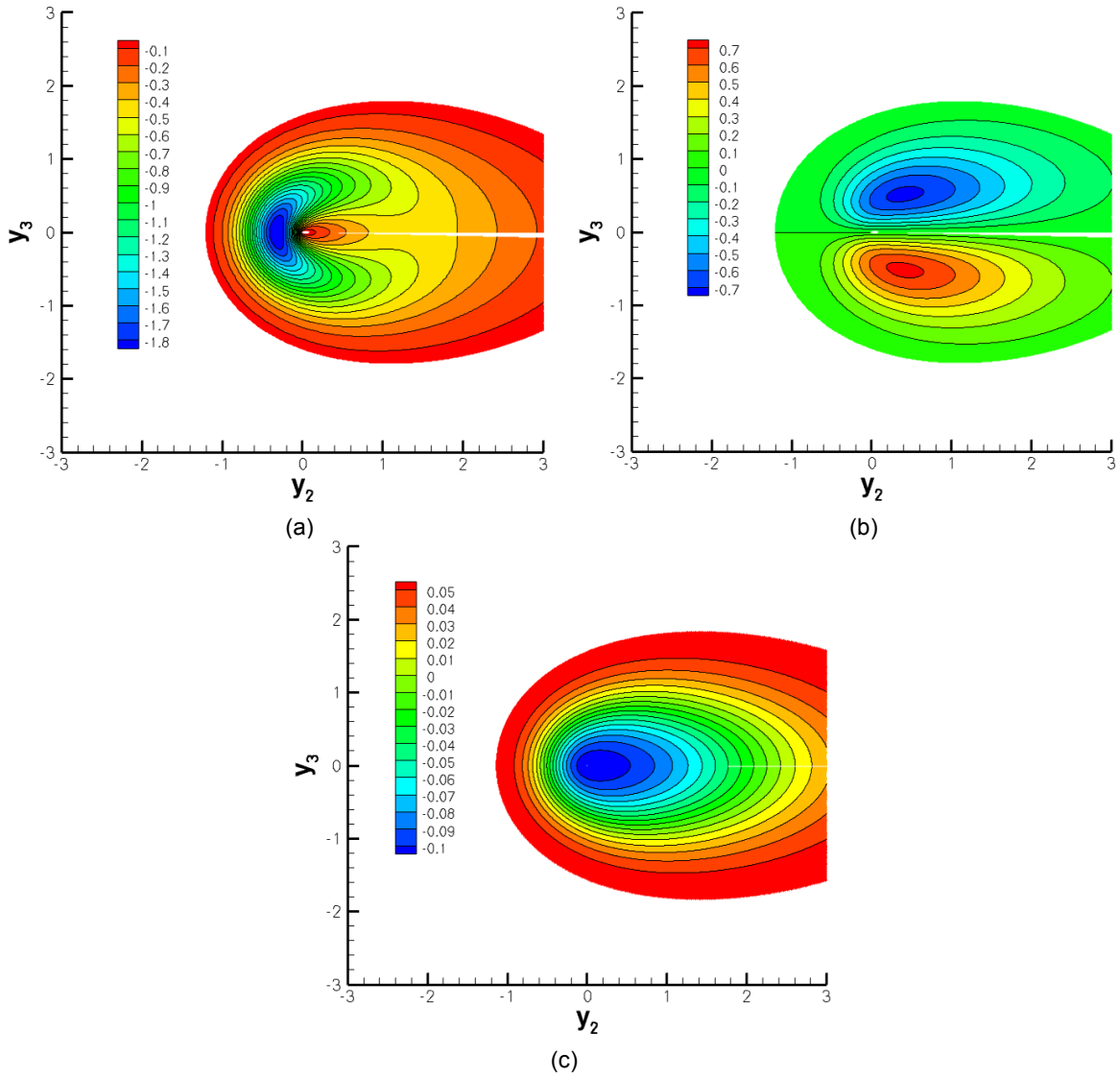

Figure 5.—Mean flow dependent coefficients of the Greens function equation for the offset jet (4.2). (a) $\mathcal{R}$, (b) $\mathcal{I}$, and (c) $\mathcal{H}$. θ = 30°.

In Figure 6 we show these quantities, and the acoustic Mach number profile, M, as functions of the azimuthal coordinate, φ, at a radial location of $r = 0.5$ and a polar angle of 30° from the jet centerline, along with their Fourier reconstructions using four, six and eight modes in (2.7).

As seen in Figure 6, the mean flow Mach number profile, and the mean flow dependent coefficients of Equation (2.3), are well represented by six modes in their respective Fourier series for this case. Results computed for the Green's function for this case, using these Fourier representations for the coefficients, are presented in the next subsection.

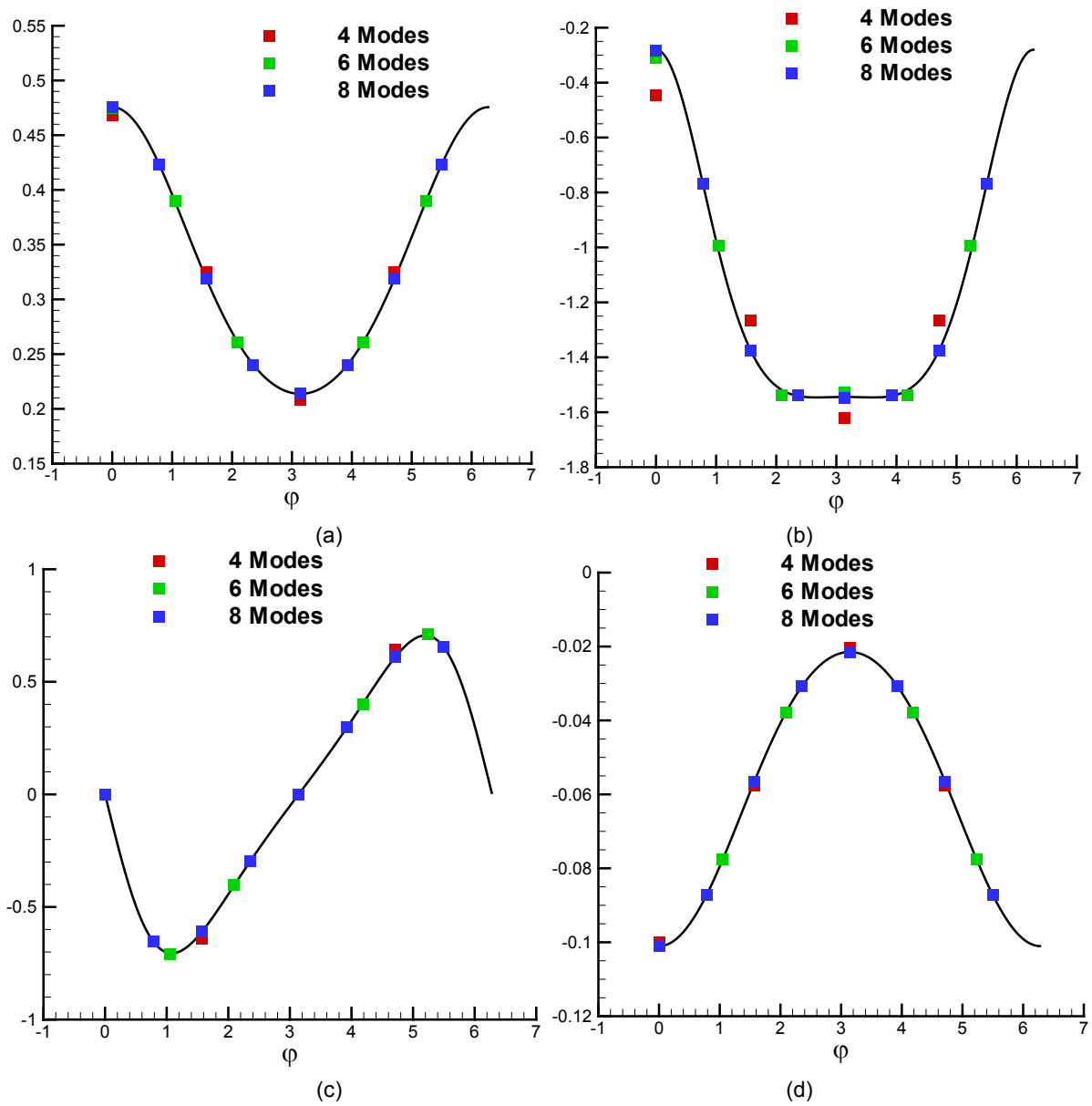

Figure 6.—Fourier series reconstruction of the mean flow terms for the offset jet. (a) M; (b) $\mathcal{R}$, (c) $\mathcal{I}$, and (d) $\mathcal{H}$.

5.1.2 Results for the Green's Function

Figure 7 shows results computed for the real (a) and imaginary (b) parts of the far-field Green's function at an observer location of 30° polar angle and 0° azimuthal angle for three radial locations in the jet. On each plot is shown results computed for the Green's function using four, six and eight Fourier modes to represent the coefficients of the governing equation and five values of the Strouhal number. As Figure 7 shows, at low Strouhal number (black and red curves), results computed using only four modes for the mean flow terms appear to be sufficient for convergence, whereas as the Strouhal number increases (blue and orange curves), a larger number is needed. The results in Figure 7 (and those computed at other observation locations but not shown here) suggest that convergence is generally reached with eight mean flow modes. The results do not converge uniformly with radial location, however; since the mean flow is relatively axisymmetric near the centerline, fewer modes are needed near the centerline (left most plots), whereas at intermediate radial locations (center plots), where there is greater asymmetry, convergence is slower.

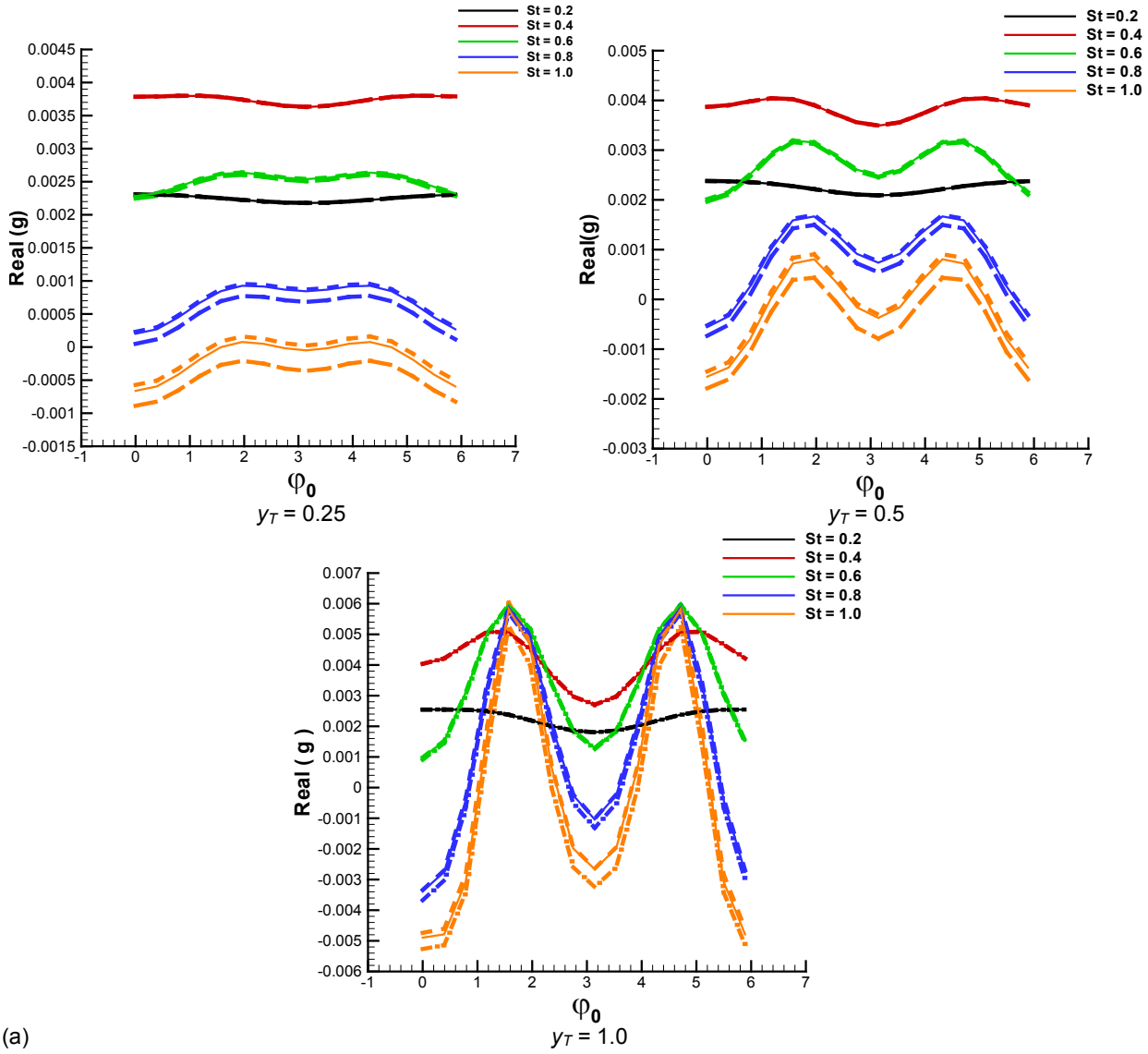

(a)

Figure 7.—Results for the (a) real part and (b) imaginary part of the Green's function versus azimuthal source location at three radial source locations using different numbers of Fourier modes for the mean flow dependent coefficients. Long-dashed L = 4; short-dashed L = 6; solid L = 8. θ = 30°, φ = 0°.

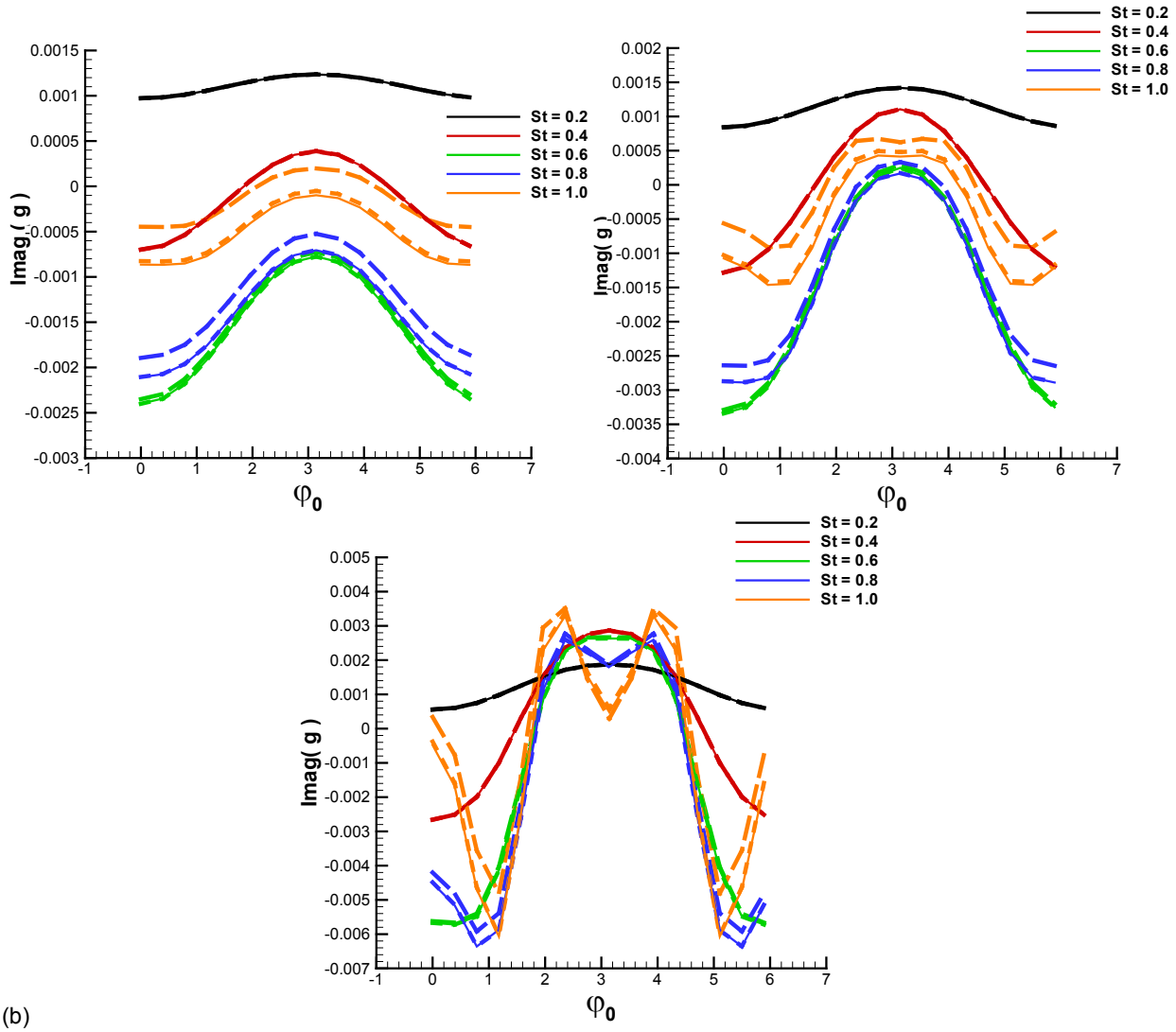

(b)

Figure 7.—Concluded.

The plots in Figure 8 show results for the scaled Green's function, $\omega^{-3/2}|g|$, versus observer azimuthal angle, at fixed source locations, for increasing Strouhal number. These results are shown at a polar angle of 60° from the jet axis, since, for this Mach number, a polar angle of 30° lies in the 'zone of silence' for the high-frequency solution. As required by the high-frequency asymptotic form of the solution, the curves are seen to eventually collapse and become independent of frequency by a Strouhal number of around two.

Figure 9 and Figure 10 are polar plots of the magnitude of the scalar adjoint Green's function versus $\varphi_0 - \varphi$ for observer polar angles of 60° and 30°, respectively, for a radial source location $y_T = 0.5$, and Strouhal numbers ranging from 0.2 to 1.0. As noted previously, for an axisymmetric mean flow the solution depends only on the difference between source and observer azimuthal locations, and in this case the curves in these figures would coincide. For non-axisymmetric cases they do not, and plotting in this way gives an indication of the degree of asymmetry. At the lowest frequency shown, St =0.2, the Green's function is fairly axisymmetric, although there is a slight bias toward larger values when the source is in line with the observer (i.e., at $\varphi_0 - \varphi = 0$) at $\theta = 30°$(Figure 10(a)) particularly for $\varphi = \pi$. As the frequency increases, however, there is significant asymmetry in the Green's function. The largest asymmetry appears to occur at $\theta = 30°$and for $\varphi = 0°$.

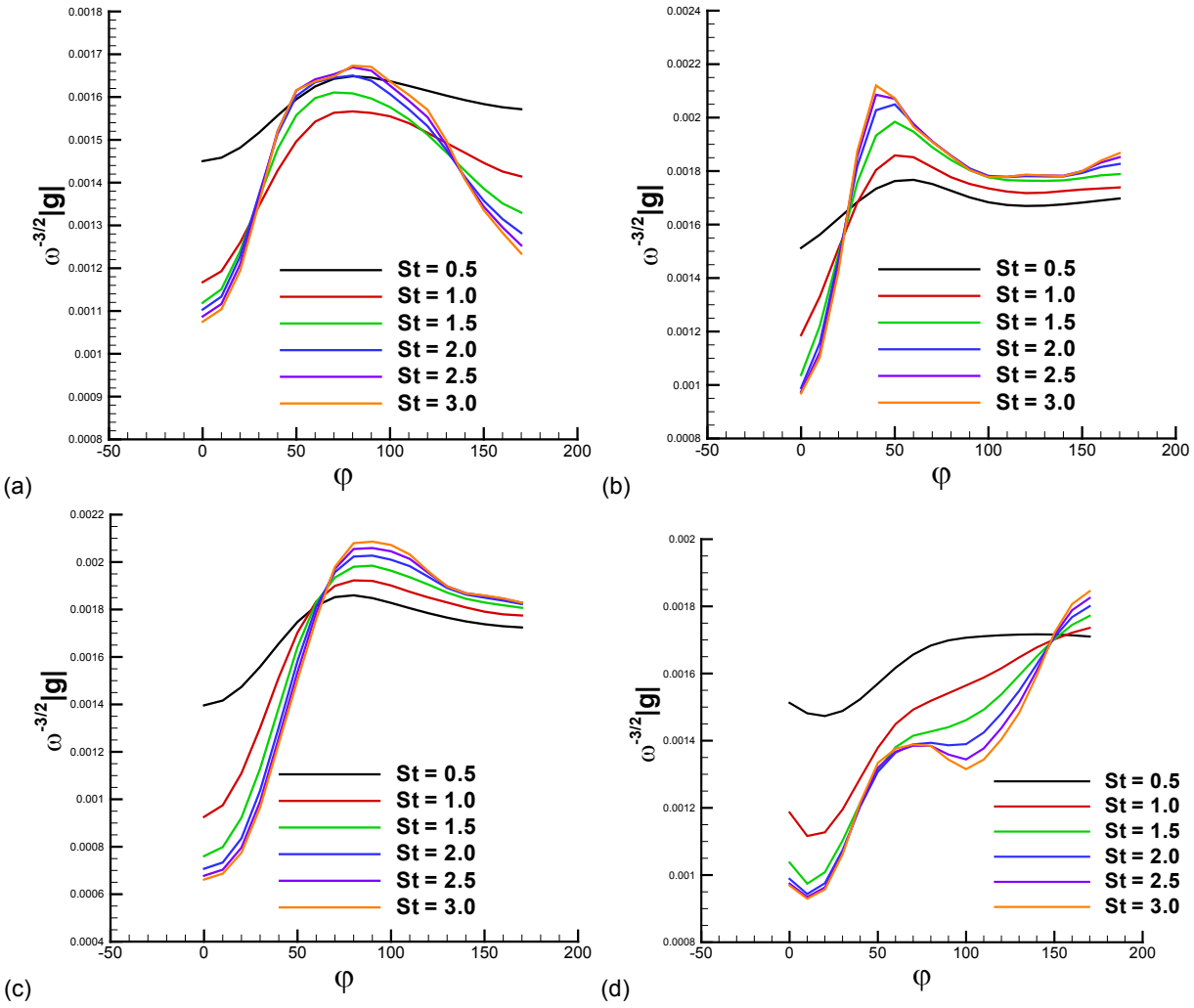

Figure 8.—Collapse of the scaled Green's function with increasing St – Offset jet. $\theta = 60°$, $y_T = 0.5$; (a) $\varphi_0 = 0°$, (b) $\varphi_0 = 90°$, (c) $\varphi_0 = 180°$, and (d) $\varphi_0 = 270°$.

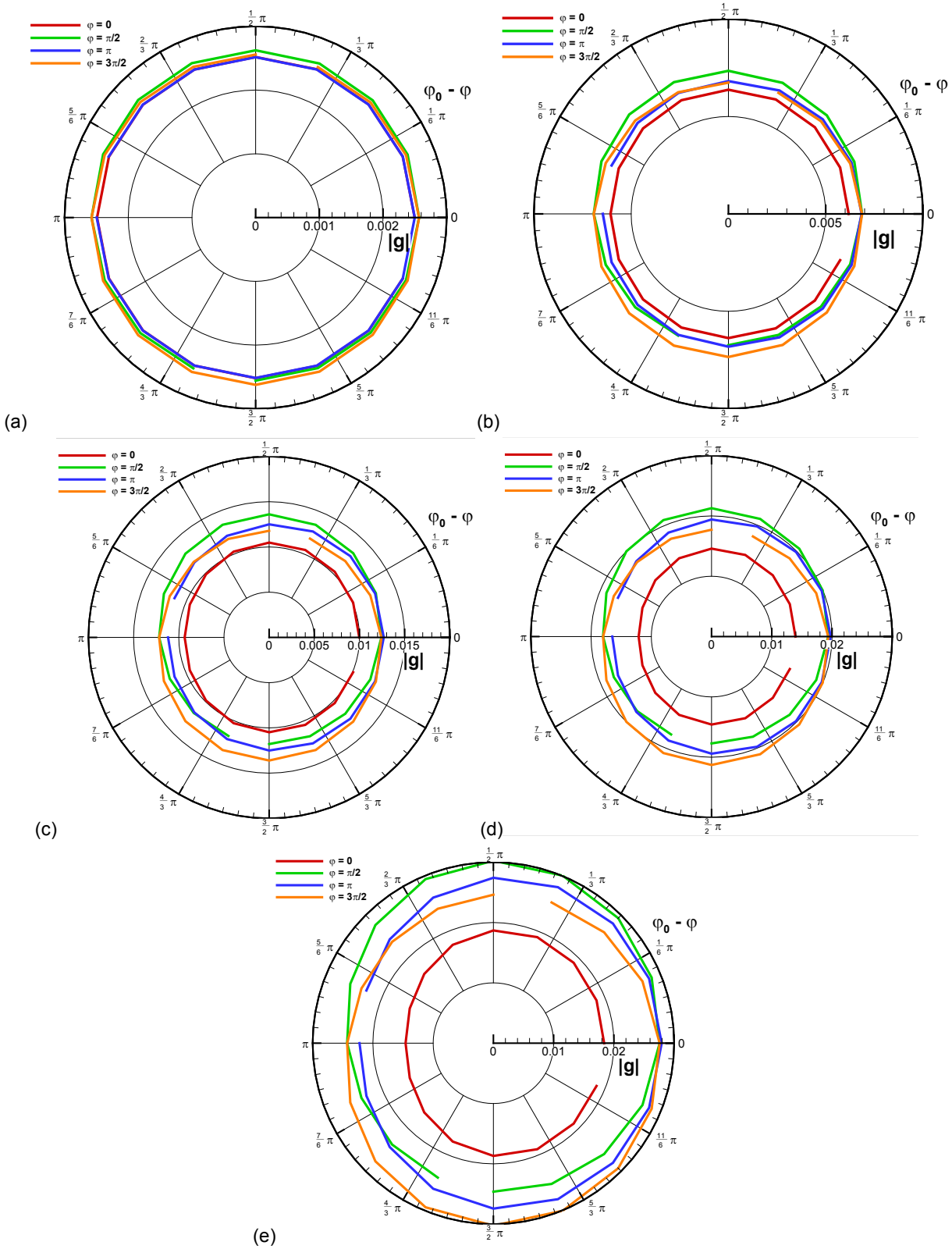

Figure 9.—Polar plots of $|g(y_T, \varphi_0; \varphi, \theta : \omega)|$ versus $\varphi_0 - \varphi$ at $y_T = 0.5$ for $\theta = 60°$ for the offset jet. (a) St = 0.2; (b) St = 0.4; (c) St = 0.6; (d) St = 0.8; and (e) St = 1.0.

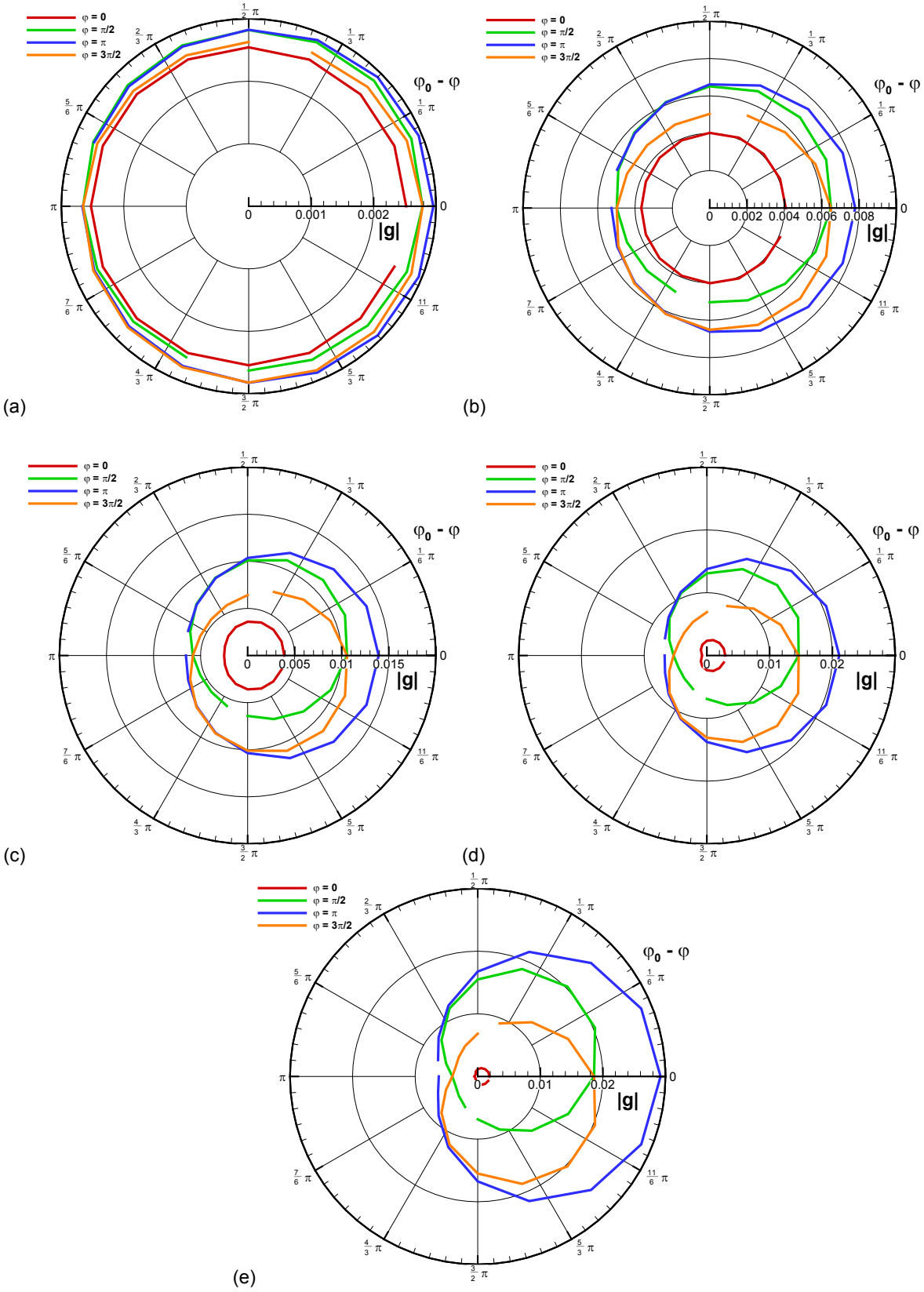

Figure 10.—Polar plots of $|g(y_T, \varphi_0; \varphi, \theta : \omega)|$ versus $\varphi_0 - \varphi$ at $y_T = 0.5$ for $\theta = 30°$. (a) St = 0.2; (b) St = 0.4; (c) St = 0.6; (d) St = 0.8; and (e) St = 1.0.

To try to get some idea of the noise shielding that may occur due to this non-axisymmetric mean flow, in Figure 11 we have selected two azimuthal observer locations, $\varphi = 0$ and $\varphi = \pi$, from the results of Figure 10 to examine in more detail. The curves shown correspond to radial source locations of $y_T = 1.0$ (b) and $y_T = 0.5$ (c). The relatively low value for the Green's function at $\varphi - \varphi_0 = 0$ for $\varphi = 0$ (red curve), relative to that for $\varphi = \pi$ (blue curve) suggests that the observer at $\varphi = 0$ (right side) is shielded from the source at $\varphi_0 = 0$ more than the observer at $\varphi = \pi$ (left side) is from the source at $\varphi_0 = \pi$. The asymmetry is larger at $y_T = 1.0$ but also quite significant at $y_T = 0.5$. Based on these results, the sound levels radiated to observer locations at $\varphi = 0°$ from a source located at $(y_T, \varphi_0) = (0.5, 0)$ could potentially be 5 dB lower than that radiated to $\varphi = \pi$ from a source located at $(y_T, \varphi_0) = (0.5, \pi)$. The differences at a radial location of $y_T = 1.0$ is more like 15 dB, but it should be noted that the turbulence levels will probably be quite low at such a relatively distant radial location from the jet centerline, and the importance of these source locations would therefore be diminished. It is emphasized again that the magnitude of the Green's function itself is not the only factor in determining the azimuthal directivity of the sound field in a non-axisymmetric jet and that these results are illustrative only.

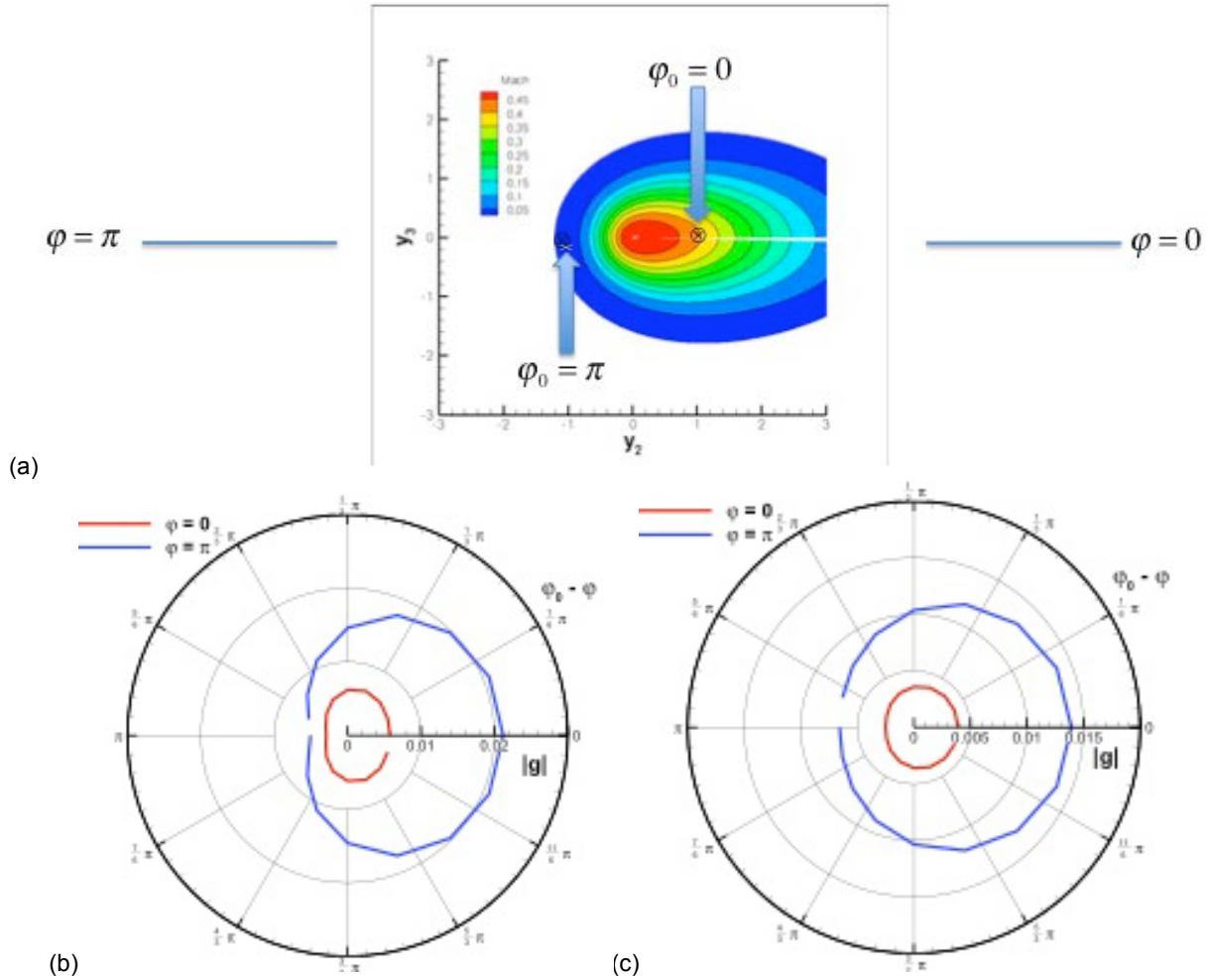

Figure 11.—Shielding of sound by the mean flow to two observer locations from two source locations—Offset Jet. St = 0.6.

5.2 Fluid Shield

5.2.1 Fourier Representation of the Mean Flow Terms

Results for the Fourier series representation of the mean flow terms appearing in the governing equations for the case of the fluid shield are presented in this subsection. For this geometry, the mean acoustic Mach number profile is given by (4.3), and again a uniform mean sound speed is used. Contour plots in the cross flow, (y_2, y_3), plane for, $\mathcal{R}$, $\mathcal{I}$, $\mathcal{H}$, in Equation (2.3) are shown in Figure 12 for this case.

The mean flow for this case is somewhat more asymmetric than the offset jet considered above, and we might expect that it would require more Fourier modes to adequately represent these quantities in this case. In Figure 13 we show these quantities, and the acoustic Mach number profile, M, as functions of the azimuthal coordinate, φ, at a radial location of $r = 0.5$ and a polar angle of 30° from the jet centerline, along with their Fourier reconstructions using four, eight and twelve modes in (2.7).

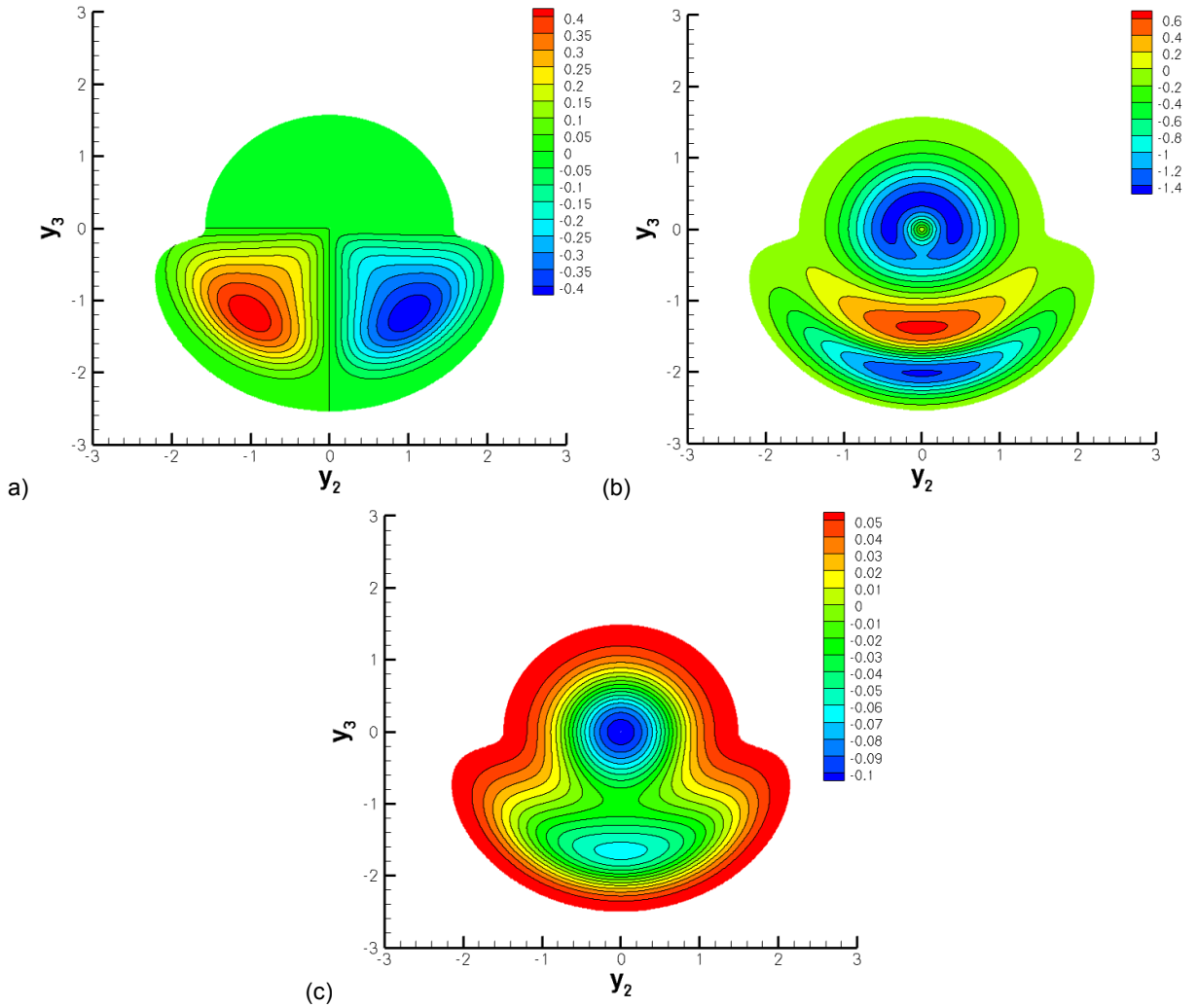

Figure 12.—Mean Flow Quantities—Fluid Shield. (a) $\mathcal{R}$; (b) $\mathcal{I}$ and (c) $\mathcal{H}$. θ =30°

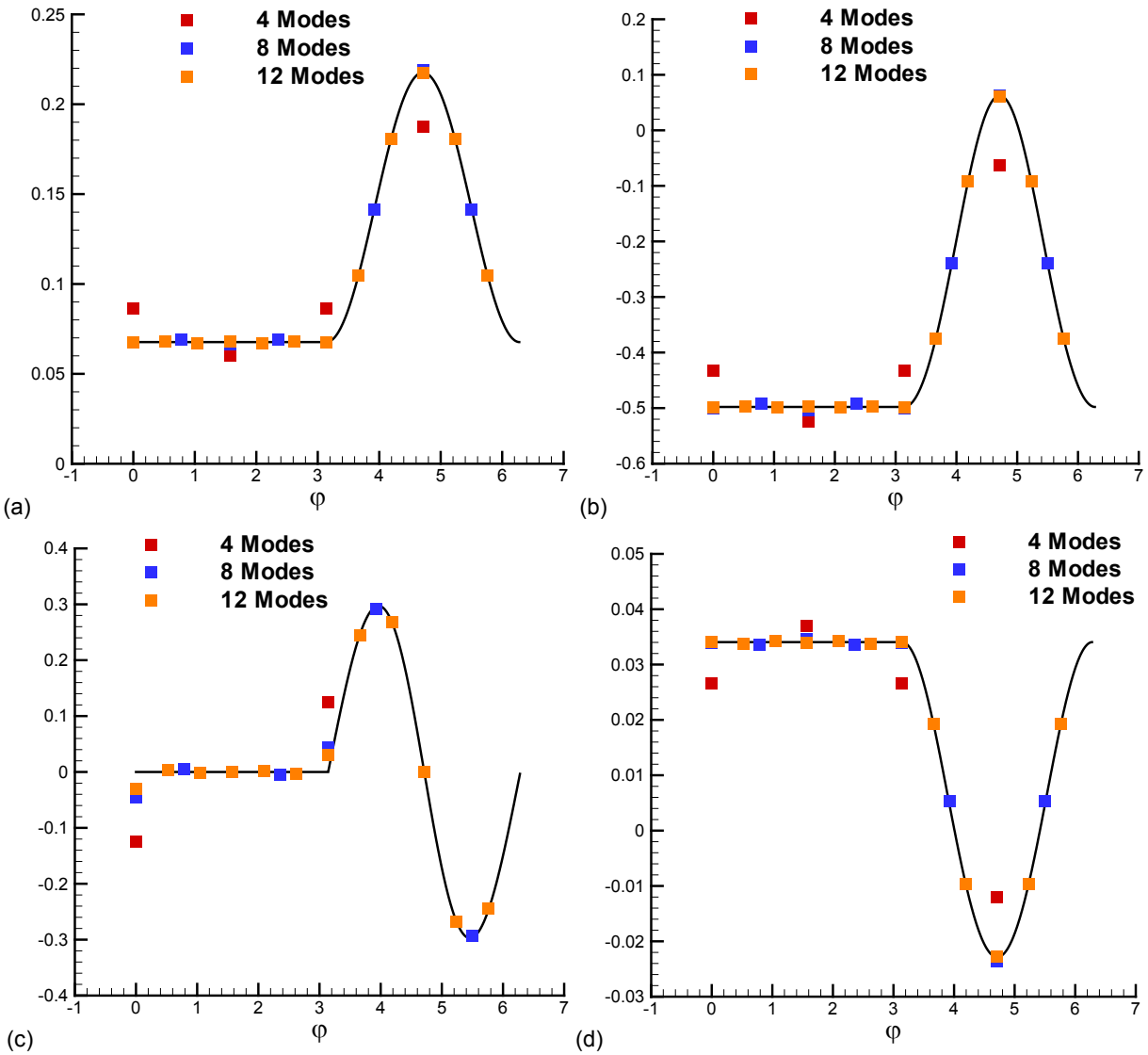

Figure 13.—Fourier reconstruction of the mean flow terms for the fluid shield. (a) M; (b) $\mathcal{R}$; (c) $\mathcal{I}$; and (d) $\mathcal{H}$.

As expected, the results in Figure 13 show that for this (more asymmetric) case, a larger number of Fourier modes, generally eight, is needed to adaquately represent the mean flow terms.

5.2.2 Green's Function

In this section we present results for the Green's function for the fluid shield. Figure 14 shows results computed for the real (a) and imaginary (b) parts of the far-field Green's function at an observer location of 30° polar angle and 0° azimuthal angle for three radial locations. On each plot is shown results computed using four, six and eight Fourier modes to represent the coefficients of the governing equation and five values of the Strouhal number. For this case, even though the mean flow is more asymmetric than the offset jet, it appears that using only four modes for the mean flow terms is sufficient for convergence of the Green's function, up to a Strouhal number of one.

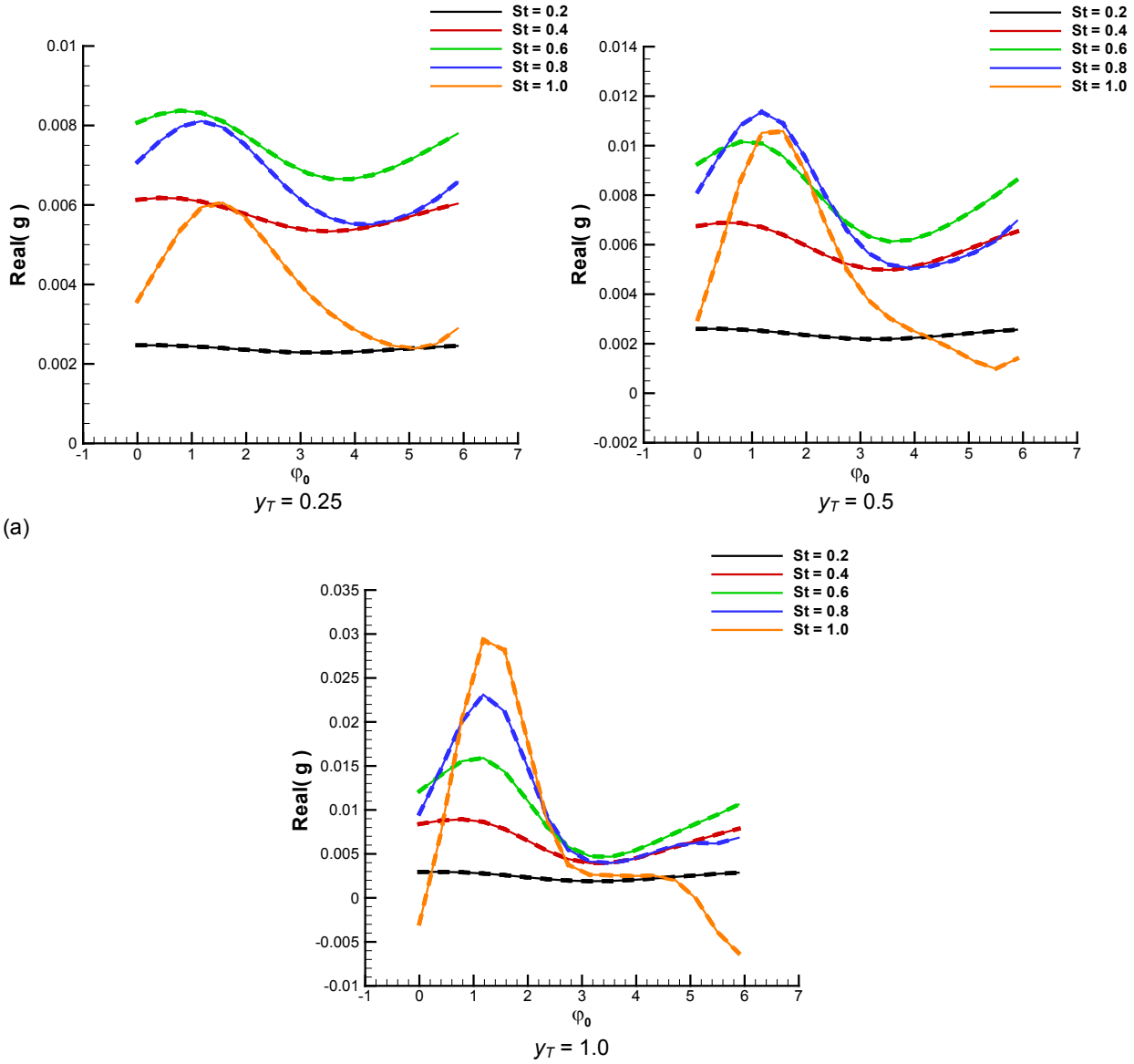

(a)

Figure 14.—Results for the (a) real part and (b) imaginary part of the Green's function versus azimuthal source location at three radial source locations using different numbers of Fourier modes for the mean flow dependent coefficients. Long-dashed L = 4; Short-dashed L = 6; solid L = 8. θ = 30°, φ = 0°.

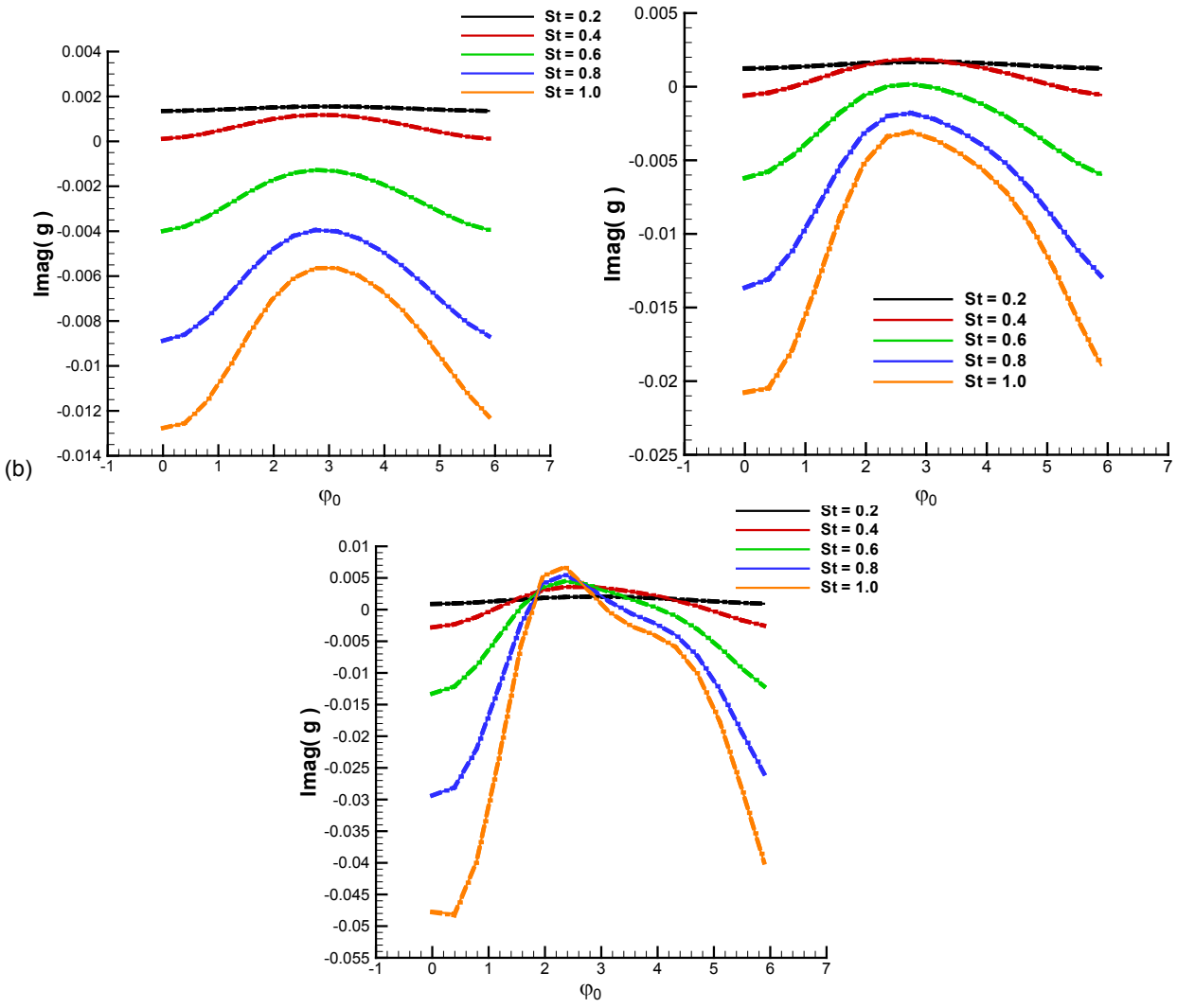

Figure 14.—Concluded.

Figure 15 shows results for the scaled Green's function, $\omega^{-3/2}|g|$, at a fixed source location as the Strouhal number is increased. A slightly higher Strouhal number (around 2.5) is needed for these curves to collapse compared with the offset jet case, but the required frequency independence is also achieved in this case.

Figure 16 and Figure 17 are polar plots of the magnitude of the scalar adjoint Green's function versus $\varphi_0 - \varphi$ for observer polar angles of 60° and 30°, respectively, corresponding to radial source location, $y_T = 0.5$ and Strouhal numbers ranging from 0.2 to 1.0 for the fluid shield case. As was found in the offset jet case, at the lowest frequency shown, St =0.2, the Green's function is fairly axisymmetric, and there is greater asymmetry at $\theta = 30°$ relative to that at $\theta = 60°$. Also, as the frequency increases there is again significant asymmetry in the Green's function.

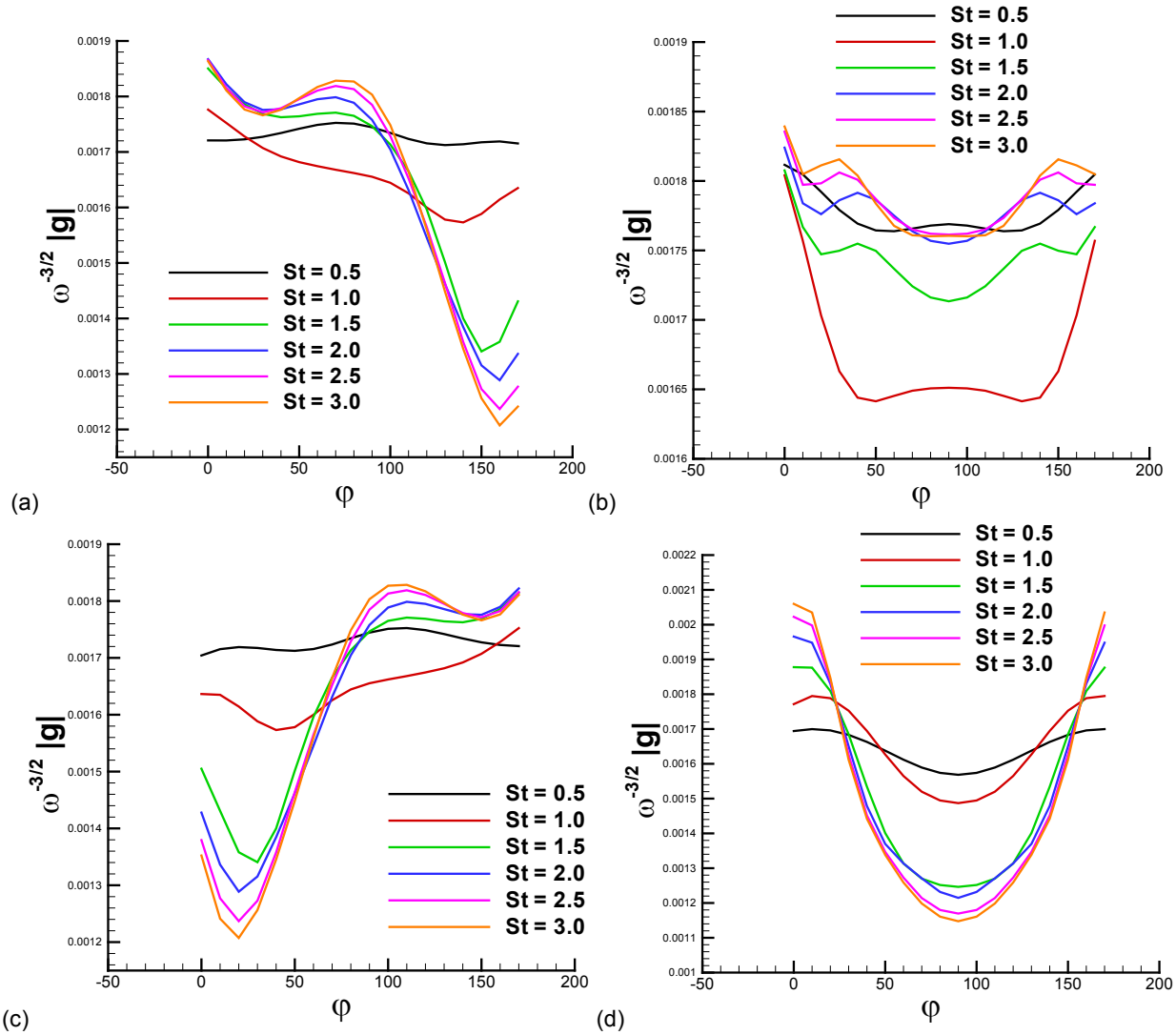

Figure 15.—Collapse of scaled Green's function with increasing St—Fluid Shield. $\theta = 60°$, $y_T = 0.5$; (a) $\varphi_0 = 0°$, (b) $\varphi_0 = 90°$, (c) $\varphi_0 = 180°$, and (d) $\varphi_0 = 270°$.

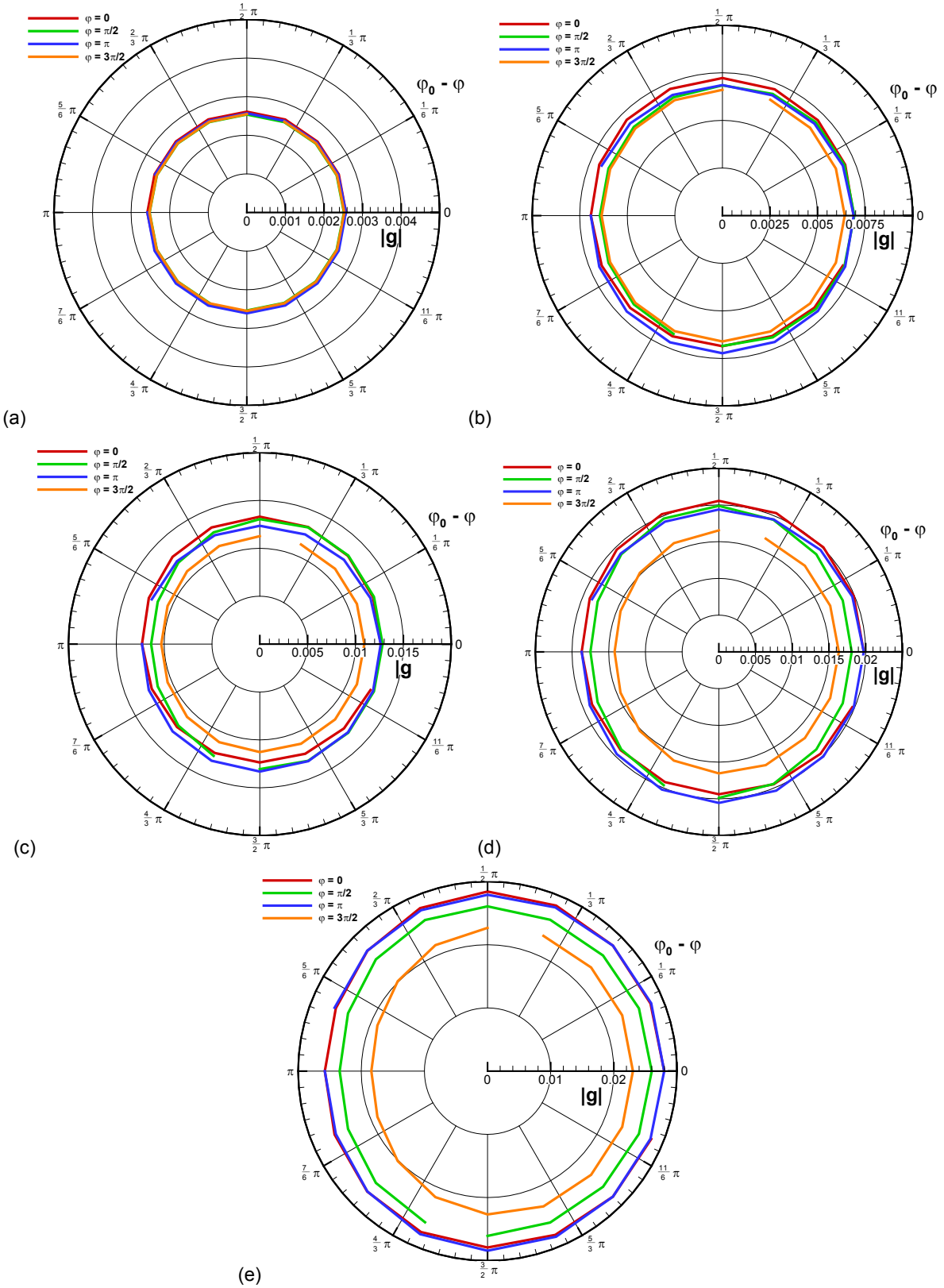

Figure 16.—Polar plots of $|g(y_T, \varphi_0; \varphi, \theta : \omega)|$ versus $\varphi_0 - \varphi$ at $y_T = 0.5$ for $\theta = 60°$ for the fluid shield. (a) St = 0.2; (b) St = 0.4; (c) St = 0.6; (d) St = 0.8; and (e) St = 1.0.

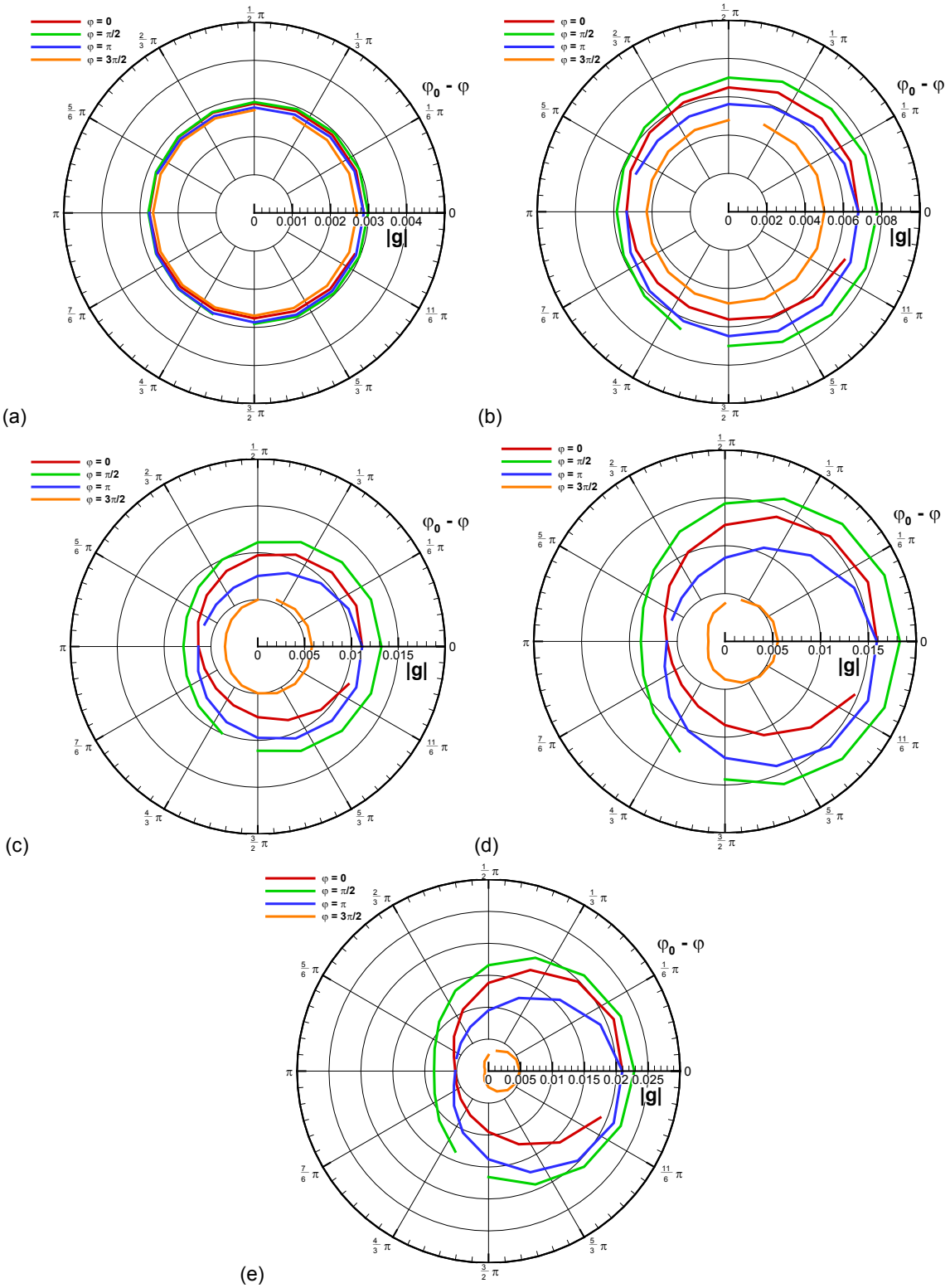

Figure 17.—Polar plots of $|g(y_T, \varphi_0; \varphi, \theta : \omega)|$ versus $\varphi - \varphi_0$ at $y_T = 0.5$ for $\theta = 30°$ for the fluid shield. (a) St = 0.2; (b) St = 0.4; (c) St = 0.6; (d) St = 0.8; (e) St = 1.0.

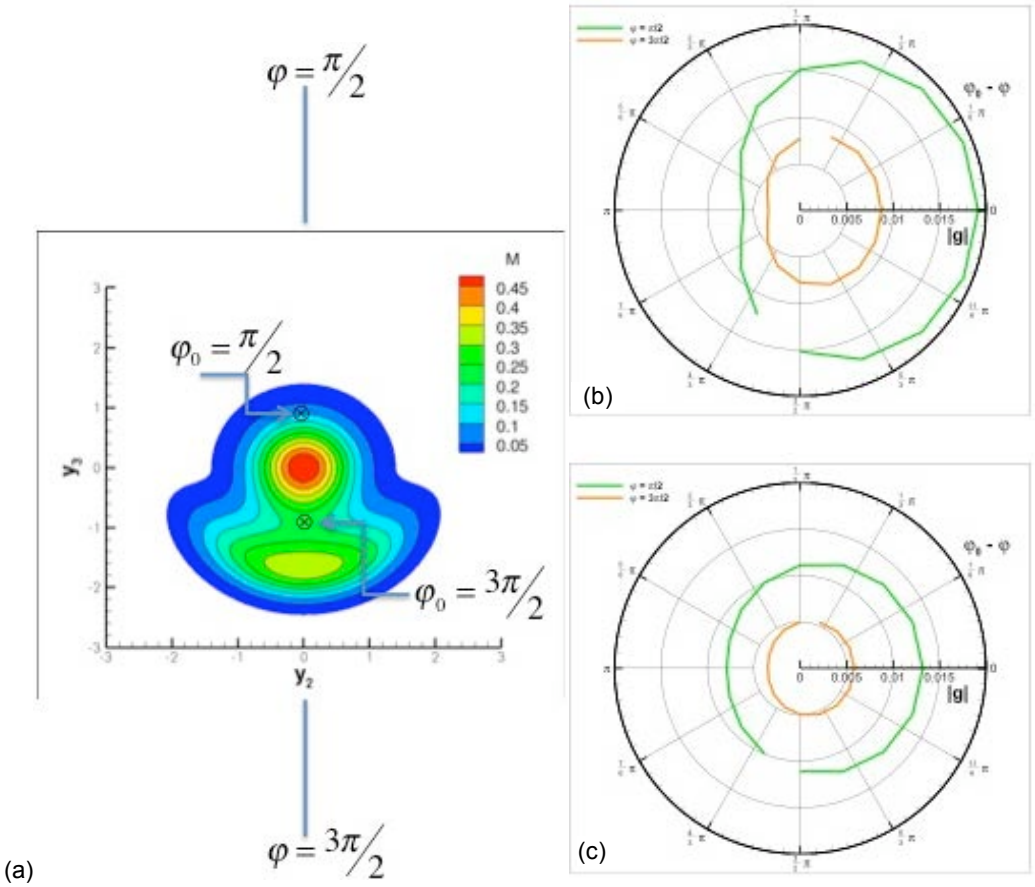

Figure 18.—Shielding of sound by the mean flow to two observer locations from two source locations—Fluid Shield. St = 0.6.

As for the case of the fluid shield, we have selected two azimuthal observer locations, $\varphi = \pi/2$ and $\varphi = 3\pi/2$ here, from the results of Figure 17 to examine in more detail. The curves shown in Figure 18 again correspond to radial source locations of $y_T = 1.0$ (b) and $y_T = 0.5$ (c). The relatively low value for the Green's function magnitude at $\varphi - \varphi_0 = 0$ for $\varphi = 3\pi/2$ (yellow curve), relative to that for $\varphi = \pi/2$ (green curve) suggests that the observer at $\varphi = 3\pi/2$ (bottom) is shielded from the source at $\varphi_0 = 3\pi/2$ more than the observer at $\varphi = \pi/2$ (top) is from the source at $\varphi_0 = \pi/2$, suggesting that the partial secondary stream does in fact act like a noise shield for source locations below the core stream. The asymmetry is again more pronounced at $y_T = 1.0$ than at $y_T = 0.5$, but to a somewhat lesser extent than for the offset jet case.

6.0 Summary and Conclusions

In this report we have documented a numerical method for computing the far-field scalar adjoint Green's function of the acoustic analogy equations for a locally parallel, non-axisymmetric, mean flow. A computer code was written to implement this method and we have reported here on its validation and on the results for a set of sample test cases chosen for relevance to certain noise-reduction concepts of current interest. The method relies on a Fourier series representation of the azimuthal variation of the mean flow depenedent coefficients appearing in the governing equation for the Green's function, and solves for the latter in terms of its own azimuhal Fourier components.

The method was initially validated by using it to compute the Green's function for a round jet and comparing the results with those obtained from an exisitng round jet noise prediction code.

It was demonstrated, for the two non-axisymmetric test cases examined, that the mean flow dependent coefficients appearing in the governing equation for the Green's function can be represented by a reasonably small number of Fourier modes—an important result for the viability of the method and its potential use in jet noise predictions. The effect of the number of Fourier components used to represent the mean flow on the numerical solution for the Green's function was tested and the number of modes needed for convergence of the results was also found to be relatively small for the two test cases considered. It was also verified that the appropriately scaled Green's function becomes independent of frequency as the Strouhal number becomes large, as the high-frequency asymptotic solution suggests.

The azimuthal directivity characteristics of the Green's function for the two test cases considered here were examined and results for a pair of azimuthal observer locations for each case were considered in a bit more detail to try to glean some information about the noise shielding potential of the respective non-axisymmetric mean flows.

For a complete noise prediction, of course, the Green's function solver described in this report must be combined with appropriate models for the source terms, with the mean flow and turbulence quantities being supplied by a Reynolds-averaged Navier-Stokes (RANS) solution for the flow. Based on the results obtained for the two test cases considered in this report, it appears that the numerical method developed here could be used in more realistic mean flow profiles and incorporated into a noise prediction scheme for non-axisymmetric jets. The next steps in the development of a noise prediction method based on this Green's function solver include extending the routines that carry out the Fourier series decomposition of the mean flow terms to handle profiles from a RANS solution and its integration with an appropriate source model.

References

1. Lighthill, M.J., "On Sound Generated Aerodynamically: I. General Theory," *Proc. R Soc. Lond.*, A211, pp. 546-587, 1952.
2. Lighthill, M.J., "On Sound Generated Aerodynamically: II. Turbulence as a Source of Sound," *Proc. R Soc. Lond.*, A222, pp. 1-32, 1954.
3. Lilley, G.M., "On the Noise From Jets," AGARD-CP-131, pp. 131-132, 1974.
4. Khavaran, A., Bridges, J. and Georgiadis, N., "Prediction of Turbulence-Generating Noise in Jets," NASA/TM—2002-211696.
5. Dahl, M.D. (ed.) "Assessment of NASA's Aircraft Noise Prediction Capability," NASA/TP—2012-215653, Bridges, J.E., Khavaran, A. and Hunter, C.A., Chapter 8—Jet Noise Prediction.
6. Goldstein, M.E., "A Generalized Acoustic Analogy," *Journal of Fluid Mechanics,* Vol. 488, pp.315-333, 2003.
7. Goldstein, M.E. and Leib, S.J., "The Aeroacoustics of Slowly Diverging Supersonic Jets," *Journal of Fluid Mechanics,* Vol. 600, pp. 291-337, 2008.
8. Leib, S.J. and Goldstein, M.E. "Hybrid Source Model for Predicting High-Speed Jet Noise," *AIAA Journal*, Vol. 49, No. 7, 2011.
9. Leib, S.J. "Noise Predictions for Rectangular Jets Using a Conformal Mapping Method, "*AIAA Journal*, Vol. 51, No. 3, pp. 721-737.
10. Frate, F.C. and Bridges, J.E., "Extensible Rectangular Nozzle Model System," AIAA paper 2011-975.
11. Zaman, K.B.M.Q, "Flow-Field Surveys for Rectangular Jets," NASA/TM—2012-217410, 2012.
12. Bridges, J.E. and Wernet, M.P., "Turbulence Measurements of Rectangular Nozzles with Bevel," Extended abstract for 19th AIAA/CEAS Aeroacoustics Conference, May 27-29 2013.
13. Bridges, J.E., "Acoustic Measurements of Rectangular Nozzles with Bevel," AIAA paper 2012-2252.
14. Goldstein, M.E. 1982 "High Frequency Sound Emission from Moving Point Multipole Sources Embedded in Arbitrary Transversely Sheared Mean Flows." *Journal of Sound and Vibration*, Vol. 80, No. 4, pp. 499-522.

REPORT DOCUMENTATION PAGE	Form Approved OMB No. 0704-0188

1. REPORT DATE *(DD-MM-YYYY)*	2. REPORT TYPE	3. DATES COVERED *(From - To)*
01-03-2014	Final Contractor Report	

4. TITLE AND SUBTITLE
Modeling Sound Propagation Through Non-Axisymmetric Jets

5a. CONTRACT NUMBER
NNC07BA13B

5b. GRANT NUMBER

5c. PROGRAM ELEMENT NUMBER

6. AUTHOR(S)
Leib, Stewart, J.

5d. PROJECT NUMBER

5e. TASK NUMBER

5f. WORK UNIT NUMBER
WBS 984754.02.07.03.17.06

7. PERFORMING ORGANIZATION NAME(S) AND ADDRESS(ES)
Ohio Aerospace Institute
22800 Cedar Point Road
Brook Park, Ohio 44142

8. PERFORMING ORGANIZATION REPORT NUMBER
E-18827

9. SPONSORING/MONITORING AGENCY NAME(S) AND ADDRESS(ES)
National Aeronautics and Space Administration
Washington, DC 20546-0001

10. SPONSORING/MONITOR'S ACRONYM(S)
NASA

11. SPONSORING/MONITORING REPORT NUMBER
NASA/CR-2014-218107

12. DISTRIBUTION/AVAILABILITY STATEMENT
Unclassified-Unlimited
Subject Categories: 01 and 07
Available electronically at http://www.sti.nasa.gov
This publication is available from the NASA Center for AeroSpace Information, 443-757-5802

13. SUPPLEMENTARY NOTES

14. ABSTRACT
A method for computing the far-field adjoint Green's function of the generalized acoustic analogy equations under a locally parallel mean flow approximation is presented. The method is based on expanding the mean-flow-dependent coefficients in the governing equation and the scalar Green's function in truncated Fourier series in the azimuthal direction and a finite difference approximation in the radial direction in circular cylindrical coordinates. The combined spectral/finite difference method yields a highly banded system of algebraic equations that can be efficiently solved using a standard sparse system solver. The method is applied to test cases, with mean flow specified by analytical functions, corresponding to two noise reduction concepts of current interest: the offset jet and the fluid shield. Sample results for the Green's function are given for these two test cases and recommendations made as to the use of the method as part of a RANS-based jet noise prediction code.

15. SUBJECT TERMS
Aeronautics; Aeroacoustics

16. SECURITY CLASSIFICATION OF:			17. LIMITATION OF ABSTRACT	18. NUMBER OF PAGES	19a. NAME OF RESPONSIBLE PERSON
a. REPORT	b. ABSTRACT	c. THIS PAGE			STI Help Desk (email:help@sti.nasa.gov)
U	U	U	UU	34	19b. TELEPHONE NUMBER *(include area code)* 443-757-5802